Fall 12-17-2016

On Frequency Variation of Dynamic Resting-state Functional Brain Network Activation and Connectivity with Applications to both Healthy and Clinical Populations

Maziar Yaesoubi

Maziar Yaesoubi

Candidate

Electrical and computer engineering

Department

This dissertation is approved, and it is acceptable in quality and form for publication:

Approved by the Dissertation Committee:

Vince D. Calhoun , Chairperson

Robyn L. Miller

Erik B. Erhardt

Manel Martinez-Ramon

On Frequency Variation of Dynamic Resting-state Functional Brain Network Activation and Connectivity with Applications to both Healthy and Clinical Populations

by

Maziar Yaesoubi

B.Sc., Sharif University of Technology, 2006
M.S., Linköping University, 2010

DISSERTATION

Submitted in Partial Fulfillment of the
Requirements for the Degree of

Doctor of Philosophy
Engineering

The University of New Mexico

Albuquerque, New Mexico

December, 2016

Acknowledgments

First and foremost, I want to thank my advisor Dr. Vince D. Calhoun for his continuous support and advice during my Ph.D study and research. I appreciate his patience, insightful advice and ideas as well as his immense knowledge.

I also want to thank Dr. Robyn L. Miller, Dr. Eric B. Erhardt , and Dr. Manel Martinez-Ramon for agreeing to be in my thesis committee and also for raising thoughtful comments and constructive questions.

I am also grateful to be a member of the Medical Image Analysis lab at the Mind Research Network which provided me with the chance to work and collaborate with a group of smart, knowledgeable and kind people. I specially want to thank Dr. Elena A. Allen, Rogers Silva and Eswar Damaraju for their invaluable feed-back and productive discussions.

Last but not the least, I would like to thank my parents, Shahnaz and Hadi, and my brother, Reza, for their encouragement and support for my entire life.

On Frequency Variation of Dynamic Resting-state Functional Brain Network Activation and Connectivity with Applications to both Healthy and Clinical Populations

by

Maziar Yaesoubi

B.Sc., Sharif University of Technology, 2006
M.S., Linköping University, 2010

PhD., Engineering, University of New Mexico, 2016

Abstract

One of the earliest and fundamental observation in scientific study of the brain was discovering the relation between activities in different local regions of brain and some core functions of the brain. This was later followed by observing that not only local activities of regions but also synchronous activities between distributed brain regions play a key role in high-level brain functions. Synchronous activity related to the functions of the brain is commonly referred to as functional connectivity (FC) and is studied in the form of connectivity states of the brain which measure degree of interactions between distributed parts of the brain. Functional connectivity has been studied with different imaging modalities such as electroencephalogram (EEG), magnetoencephalography (MEG) and functional magnetic resonance imaging (fMRI). The latter has the advantage of having relatively higher spatial resolution

of the underlying functional regions and is our choice for the source of the data in this work. Functional connectivity analysis of the human brain in fMRI researches focuses on identifying meaningful brain networks that have coherent activity either during a task or in the resting state. These networks are generally identified either as collections of voxels whose time series correlate strongly with a pre-selected region or voxel, or using data-driven methodologies such as independent component analysis (ICA) that compute sets of maximally spatially independent voxel weightings (component spatial maps (SMs)), each associated with a single time course (TC). Recent studies of functional connectivity have shed light on new aspects of functional connectivity. For example, connectivity during a resting state (RS) of the brain had long been know to constitute a single state of connectivity and just recently it is argued that RS-connectivity, varies in time and has a dynamic nature. In this work, we investigate new aspects of RS-connectivity jointly with its dynamic aspect. As part of the new observations, we discuss that RS-connectivity is in fact frequency dependent in addition to be temporally dynamic. This discovery allows to capture RS-coonectivity at a given time as the superposition of multiple connectivity states along frequency dimension. Later, we also show that interaction between fMRI networks is not only frequency dependent and temporally dynamic but also may occur cross different frequency spectra which is the first evidennce of cross-frequency depenence between fMRI functional networks. We also discuss that all of these observations would enable us to design novel measures to explain RS-connectivity variation among different group of subjects such as healthy and diseased or males and females which would have clinical diagnosis applications and could possibly serve as new bio-markers to study underlying functions of the brain.

Contents

List of Figures

Chapter 1

Introduction

1.1 Overview

One of the very first and fundamental observation of human brain was that its function is the result of integration of activities of local regions which are distributed over the brain. Each of these distributed regions has been associated to specific functions of the brain which have been refined over time [2]. For example in early 19th century, through experim1ental brain ablations, scientists could distinct functions of cerebrum ad cerebellum and now with advancements of non-invasive imaging techniques we have access to a finer distinction of brain regions [3]. The association between local and distributed regions of the brain and specific brain functions is known as *functional segregation* aspect of the brain [4] (Figure 1.1 A).

Moreover, integration aspect of the brain has been investigated by studying coherent regional activities wildly referred to as *brain connectivity* . In fact it has been observed that not only local activation of brain regions but also synchronous activities between set of regions contribute to execution of higher level functions of the brain. Coherent activity of distributed brain regions is widely referred to as

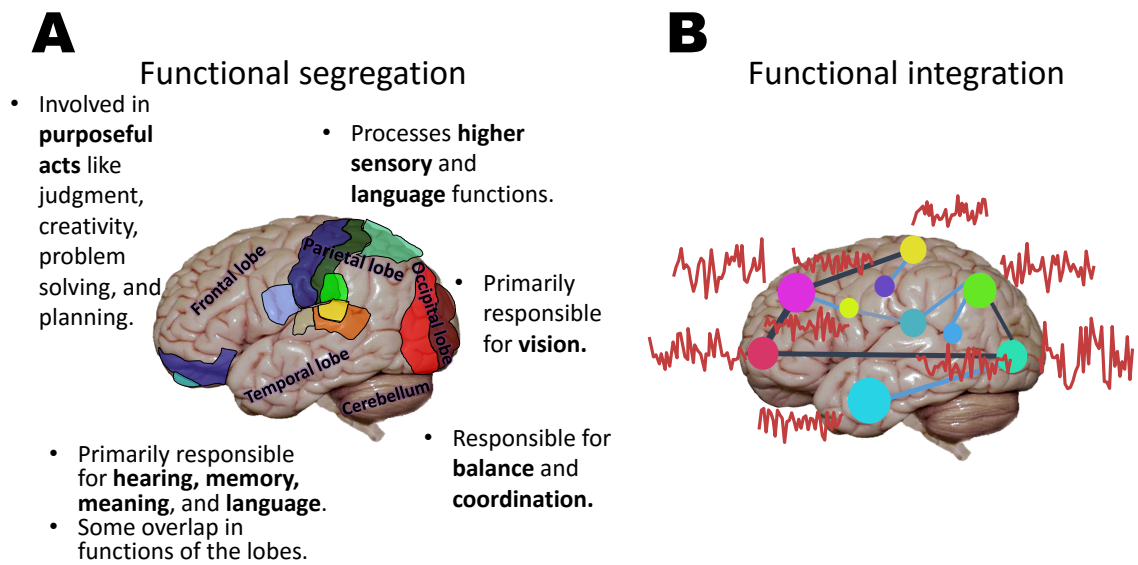

Figure 1.1: (A) Functional segregation versus (B) functional integration.

functional integration aspect of the brain [5] (Figure 1.1 B).

Evidences of functional integration initially evolved from functional segregation as well as the structural morphology of brain when co-activity of anatomically distant regions was observed. Knowledge on anatomical and morphological connectivity, which are usually referred to as *structural* connectivity, has been improved by introduction of tracing techniques such as *"Anterograde" (forward)* and *Retrograde (backward)* [6] tracing as well as diffusion tensor imaging (DTI) [7]. These techniques, however, capture connectivity independent of the current functional state of the brain. In fact, connectivity as the interactions of brain regions due to the function of the brain, which is known as *functional connectivity*, although is partly derived from structural connectivity, is also adapted to the current function of the brain. Neuroimaging techniques which capture functionally related activities of the brain have been used to estimate functional connectivity as a venue to study functional integration aspect of the brain. These techniques, although, measure a correlate of

the actual neuronal activity, differ based on the type of the actual signal they capture. As an example, electroencephalogram (EEG) measures voltage differences on the scalp as the result of simultaneous activity of large number of neurons. Even with state of the art EEG devices, a large number of neurons is need to sum up their activity to produce a strong signal to be picked by EEG electrodes. Moreover since EEG picks the signal on the scalp, an inverse problem needs to be solved to localized actual sources of activity inside brain. All of this results in having poor knowledge on and low resolution of the spatial sources of activities. On the other hand, EEG electrodes are able to capture brain activities with high temporal resolution (with sampling rate of $\sim$ milliseconds). This enables EEG to capture activities in a wide range of frequencies covering known rhythmic activities of the brain including theta (4-7 Hz), alpha (7-14 Hz), beta (14-25 Hz) and gamma (low: 30-60 Hz, high: 60-100 Hz). Similar to EEG, magnetoencephalography (MEG) has advantage of having high temporal resolution but instead, it measures changes in magnetic field accompanied by the electrical activities of the brain. Similarly to EEG, MEG also suffers from having low spatial resolution although compared to EEG, its signal is attenuated less by the scalp and skull and has a slightly higher spatial resolution. However both techniques, measures brain activities with limited depth of the brain ($\sim$ 4 cm).

On the contrary, magnetic resonance imaging (MRI), has been enabled to capture volumetric images of soft tissues in different parts of the body. Particularly, MRI images captures relative population of hydrogen atoms as part of the water molecules in different parts of the body which provides a contrast between body tissues such as water and fat. This imaging technique has also been used to capture both structural and functional images of the brain. Structural MRI (sMRI) provides contrast between white matter, grey matter and cerebrospinal fluid (CSF) of the brain. In contrary to other techniques to measure of brain activity such as EEG and MEG, current MRI technology is unable to directly capture neuronal brain activities. However it was observed that, in fact, MRI can made to be sensitive to level

of deoxyhemoglobin in the veins. This observation, lead to the design of functional MRI which captures blood-oxygen-level dependent (BOLD) contrast which its local changes in the brain is known to correlate underlying neuronal activities of the brain.

1.2 Principles of BOLD signal and fMRI technology

From late 19th and early 20th century, it has been hypothesized that neuronal activity is correlated to changes in blood flow [8]. This hypothesis was later accompanied by first evidences of magnetic properties of blood [9] which is shown to be relate to whether hemoglobin carries an oxygen molecule. Oxygenated hemoglobin (Hb) is known to be diamagnetic (having zero magnetic moment) and deoxygenated hemoglobin (dHb) is known to be paramagnetic. Consequently, differences between local concentration of dHb and Hb leads to difference in homogeneity of local magnetic field of the brain. This contrast of magnetic field homogeneity is the source of the BOLD signal. Local neuronal activities increase blood flow near the pool of corresponding neurons leading to the increase of concentration of Hb [10]. Now if hydrogen nuclei of the body initially align to a strong static magnetic field ($1.5-3$T in current commonly used fMRI scanners), when their orientation of the spins changes with radio waves (RF pulse) at the appropriate frequency (Larmor frequency) and when the pulse stops, the magnetization at the new spin orientation decays and dephases as it realigns to the initial orientation. Rate of dephasing depends on the degree of homogeneity of local magnetic fields (stronger local homogeneity of magnetic field leads to slower dephasing) which is directly related to ratio of Hb and dHB and correlates to the local and instantaneous neuronal activities. fMRI data as used here is in fact measure of the dephasing as the T_2^* images.

1.3 fMRI experiment design to map neuronal activities to the brain function and behavior

Experimental designs of fMRI are mostly based on the subtraction principle. It usually consists of two types of conditions. One is the experimental condition representing a state of the brain when focused on a task of interest. Another condition is control condition representing a baseline state of the brain. Having the design, there are approaches which makes it possible relate the condition of the brain to the observed brain activation. One used approach is general linear model (GLM) which correlates task design to the activities in a given seed or region of interests (ROI) which requires a prior knowledge on the anatomically meaningful selection of the seed or ROI location (Figure 1.2 Left). There are also data-driven approaches that do not require a prior selection of the regions but are still able to decompose the capture brain data into a set of regions among which exist anatomically meaningful brain regions. Also , attached to each regions is a time-series which represent activities associated to that region. One of the most commonly method to achieve such decomposition is independent component analysis (ICA) (Figure 1.2 Right).

1.3.1 Group spatial independent component analysis

ICA decomposition as has been used in here is a group spatial ICA (gsICA). It is used to find functional networks of the input data of voxel-level time-series. Functinal networks as computer by gsICA are in fact a set of maximally spatially independent voxel weightings (component spatial maps (SMs)), each associated with a single timecourse (TC). gsICA as implemented in GIFT toolbox which has been used throughout this study has several stages: First, a subject-level principal component analysis (PCA) reduces the subject data temporal dimension by selecting subset of

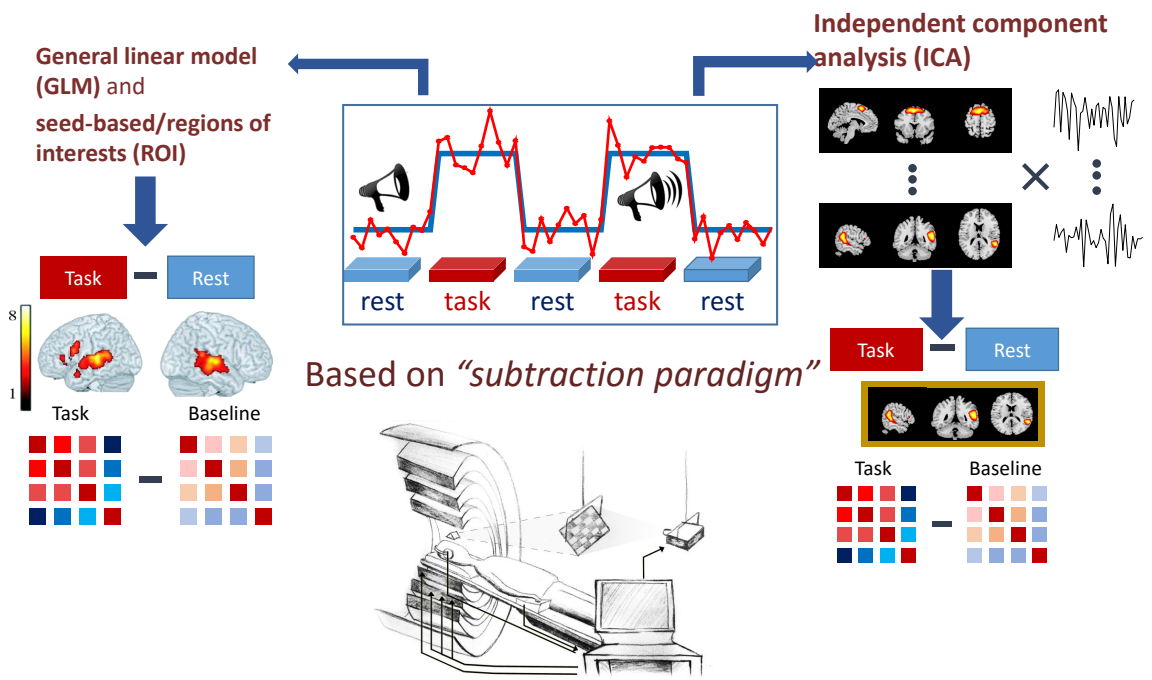

Figure 1.2: Semantic representation of a task-based experimental design. **Left:** GLM-based approaches to identify activities due to the task design in a selected ROIS. **Right:** Data-driven approaches (here based on ICA decomposition) to identify functional networks whose activities correlate to the task-design.

the principle components (PCs) explaining most of the variation of the data. This is followed by a group-level PCA on concatenated subject principal components, from which, again, a subject of PCs are retained. A set of maximally spatially independent group-level spatial maps (SMs) are obtained from this reduced group-level data using an Infomax-based algorithm. To find the most stable SMs, Infomax is repeated ten times and clustered via ICASSO [11]. The aggregate spatial maps that emerge from this process are the modes of component clusters. Note that these SMs are define at the group-level. Subject specific spatial maps and time courses can be estimated using the GICA1 [12, 13] algorithm which essentially, project subject-wise time-courses estimated from group-level analysis on the input voxel-level data for each subject to find subject-specific spatial map.

Mathematically speaking given input voxel-level data as the matrix $V_{voxel \times time} = [V^{subject\ \boldsymbol{1}}_{voxel \times time}, ..., V^{subject\ \boldsymbol{s}}_{voxel \times time}]$ where each of the $V^{subject\ \boldsymbol{i}}_{voxel \times time}$ in this implementation are pca reduced in time. ICA decompose V as follows here and visualized in Figure 1.4:

$$V_{\text{voxel}\times\text{time}} = S_{\text{voxel}\times\text{c}} \times T_{\text{c}\times\text{time}} \tag{1.1}$$

where $S_{\text{voxel}\times\text{c}}$ are the maximally independent spatial maps (ICA componnets/ brain functional networks) . The backprojection is in fact projection of $T_{\text{c}\times\text{time}} = [T^{\text{subject}\ \boldsymbol{1}}_{\text{c}\times\text{time}}, ..., T^{\text{subject}\ \boldsymbol{s}}_{\text{c}\times\text{time}}]$ on to the original input data to estmate subject-specific spatial maps as follows:

$$S^{\text{subject}\ \boldsymbol{i}}_{\text{voxel}\times\text{c}} = V^{\text{subject}\ \boldsymbol{i}}_{\text{voxel}\times\text{time}} \times T^{\text{subject}\ \boldsymbol{i}\,-1}_{\text{c}\times\text{time}} \tag{1.2}$$

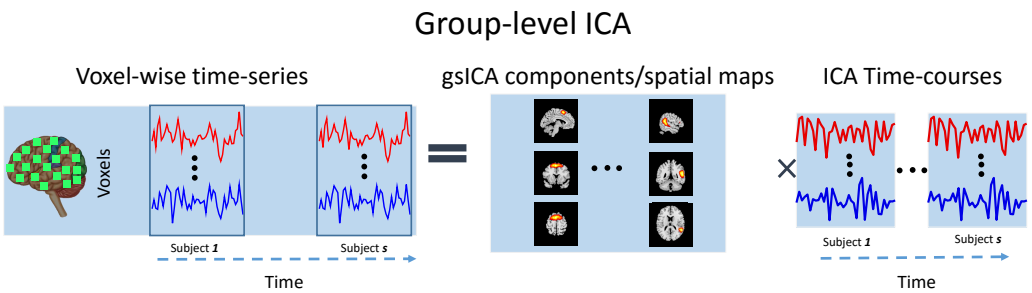

Figure 1.3: Semantic representation of ICA decomposition.

Not all estimated SMs map to actual anatomical regions of the brain by either overlapping with white-matter, known vascular or ventricular as well as components whose spatial maps overlaps the edge of the brain which is hypothesized to be susceptible to the motion. Consequently, gsICA as explained above, is usually accompanied by post-processing to remove SMs related to physiological, motion and imaging artifacts. Also additional post-processing of timecourses is usually performed, including detrending, multiple regression of the size realignment parameters and their temporal derivatives and outlier removal.

1.3.2 Resting-state experiment

Experiments solely based on resting-state of the brain has been relatively more recent compared to task-based designs. In task-based experiments, resting-state, has been mostly used as a baseline condition. However later studies showed that, in fact, brain activity, in the absence of an explicit input, is known to be spontaneous but can be correlated between functionally or structurally related regions. Variety of brain functions have been associated to the resting brain including memory and social cognition known to be related to "default mode (DM) network" of the brain (Raichle and fox 2001 a default mode of brain function pnas) which have also been identified in resting-state fMRI analysis. Other networks including somatosensory (motor and sensory), visual, auditory and language have also been identified using resting-state data along with attentional and cognitive control networks [14]. Engagement of such a variety of networks during a state of a brain which is relatively simple to perform and capture has make it appealing to a wide variety of research topics including clinical and diseased brain studies. Also since it captures a state of brain in constraint-free context, it has been shown that more variation among groups of subjects can be, consequently, observed. and lastly, it also makes it easy to study impaired subjects such as Alzheimer's patient and also to study brain in a context where there are no explicit experiment design such as hallucinations.

1.4 Objectives and contributions

Main objective of this work is to design new frameworks to study functional integration aspect of the resting-state brain in form of functional connectivity defined in a joint time and frequency domain. This enables to explore novel aspects of resting-state connectivity that have not been studied before. We also implement our proposed framework in a clinical diagnosis setting to study schizophrenia disease

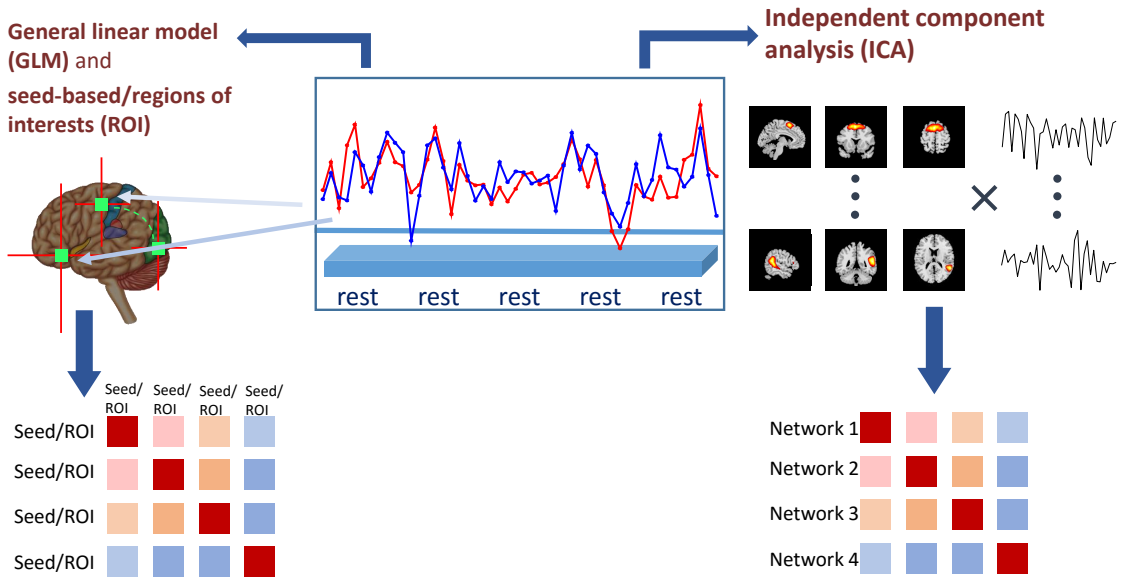

Figure 1.4: Resting state experiments with no design. In this case, data driven approaches such as ICA (right) have advantage, since by design, they do not need a prior knowledge on the design. However GLM and ROI approaches (left) can still be adapted to overcome this lack of knowledge.

and its similarities and differences from healthy control condition which are only identifiable in this augmented domain. As we will explain, resting state functional connectivity had already been studies in temporal and frequency domain but, here, for the first time, we investigate these aspect jointly in a whole brain. connectivity analysis.

1.4.1 Materials

There are two sets of the data we use in this study. First set consists of resting-state scans of 405 healthy subjects (200 females and mean age of 21.0 yeas ranging from 12 to 35 years). fMRI data was captured using the same scanner for all subjects, a 3-T Siemens Trio scanner with 12-channel radio frequency coil. T_2^*-weighted functional

images were acquired using a gradient-echo EPI sequence with TE = 29 ms, TR = 2 s, flip angle = 75°, slice thickness = 3.5 mm and gap = 1.05 mm, FOV = 240 mm, matrix size = 64x64, voxel size = 3.75 mm x 3.75 mm x 4.55 mm and informed consent was obtained according to institutional guidelines at University of New Mexico. Pre-processing steps included discarding first 4 image volumes to avoid T1 equilibration effect, realignment, slice-timing correction, spatial normalization, reslicing to 3 x 3 x 3 mm^3 voxels and Gaussian smoothing. And finally voxel time-series were z-scored to remove bias from further variance-dependent processes.

The second set of the data includes 163 healthy controls with average age of 36.9 and 151 patients diagnosed with schizophrenia with average age of 37.8. 46 of the healthy controls and 37 of patients were female. In accordance with the internal review boards of corresponding institutes, informed consent was obtained from all the subjects. fMRI scans of the subjects during a resting-state with eyes closed, were acquired across 7 different sites. Scans for each subjects constitute 162 volumes of T_2^*-weighted functional images with EPI sequence. Same scanners a 3T Siemens Tim Trio System were used in 6 sites and a 3T General Electric Discovery MR750 scanner was used in only one of the sites. All of the scans had FOV = 11x220 mm, matrix size = 64 x 64, TR = 2 s, TE = 30 ms and FA = 770. Pre-processing included head motion, slice-timing correction and spatial normalization to the Montreal Neurological Institute (MNI) template was applied to the data using SPM toolbox followed by despiking using AFNI3 to remove outliers. The BlurToFWHM algorithm as implemented in AFNI3s was used for spatial smoothing of the data and lastly all voxel-wise time series were z-scored to normalize the variance before performing group spatial independence component analysis (gsICA).

Chapter 2

Functional network connectivity of resting-state brain

Functional connectivity (FC) analysis of the brain has been the dominant approach to study temporal dependence between brain regions as a quantification of functional integration. As explained earlier, such regions are either determined from regions-of-interest (ROIs) using prior anatomical knowledge [15, 16] or through data-driven approaches, such as ICA, which looks for maximally spatially independent components [17, 18, 19]. However, regardless of the way such regions or components have been derived, both FC and its close relative functional network connectivity (FNC) -referring to FC between component timecourses estimated by ICA- have been shown to be extremely informative about the brain function [20, 21, 22].

A key feature of most connectivity analyses (FC or FNC) of resting-state brain is that the temporal dependence is evaluated globally, as a property characterizing network pairs dependence over the entire duration of a scan. Such analysis is in fact in line with previously common assumption on resting-state with being considered as a baseline and singleton reflection of function of the brain. More recent works have

indicated however that patterns of connectivity between resting-state networks are in fact highly dynamic [23] with key features obscured by averaging over whole period of time questioning common assumption of stationary RS-connectivity. Capturing dynamic aspect of connectivity, requires new methods to be developed. Proposed methods to capture dynamic connectivity, all have been limited by their underlying assumption and in the absence of a ground truth, performance of the methods can not be directly compared and consequently the choice of the method for a given study depends on the objective of the study.

As an example, there are methods based on the estimation of "phase synchronization" between given time-courses. These methods disregard correlation between amplitudes and focus on the difference between instantaneous phases of the signals. A commonly used formulation for this methods is first projection of input signal into its analytic signal representation with a Hilbert transform as follows:

$$\psi(t) = s(t) + j\tilde{s} = A(t)e^{\mathrm{J}\phi(t)} \tag{2.1}$$

where $\tilde{s}$ is Hilbert transform of input signal s as follows:

$$\tilde{s}(t) = \frac{1}{\pi} P.V. \int_{-\infty}^{\infty} \frac{s(\gamma))}{t-\gamma} d\gamma \tag{2.2}$$

and $\psi(t)$ is analytic signal. The instantaneous phase can be estimated easily as follows:

$$\phi(t) = arctan(\frac{\tilde{s(t)}}{s(t)}) \tag{2.3}$$

and simply a difference between instantaneous phases of two signal would serve as a dynamic measure of dependence [24].

A limiting assumption of this approach is that the given signal has instantaneous narrow frequency-band and not a spectrum.

Another example is referred to as spontaneous co-activation patterns (CAPs) analysis. It looks for patterns of significant simultaneous activation (as a measure

of positive dependence) or significant difference in activation (a measure of negative dependence) between sets of networks or regions [25]. Among these methods, investigations of dynamic connectivity based on computing correlations over sliding windows through the original timecourses [26, 27, 28] has been among the most commonly used approach. The popularity is partly due to its ease of implementation and interpretation of the result and also it has just one major assumption of spatial locality. It means that at a given point in time, the samples of the time-series that fall into the window defined around that point are used for estimation of instantaneous measure of dependence. One possible implementation of this pipeline which has also been commonly used for study of resting-state dynamic connectivity has been proposed by Allen et al. In their implementation, the selected window size is fixed and weighted derived from a convolution of a Gaussian and rectangular function of the size of the window. For estimation of the correlation from weighted samples in a given window, they force a sparsity on the inverse of the covariance matrix to reduce aliasing in the estimation of correlation as the result of under-sampling. Lastly, to dynamic estimation of connectivities are summarized into finite number of prototype connectivity patterns usually referred to as "connectivity states". It is based on the assumption that connectivity of the brain follows has recurring nature and consequently reducible into finite connectivity patterns. In k-means clustering has been used in their implementation of this summarization step although other reduction methods have been proposed [29, 30]. Figure 2.1 summarizes sliding-window implementation by [31].

2.1 Frequency variation of connectivity

Temporal domain has not been the only domain to study brain connectivity. Specifically, based on the common assumption that different sources of brain activities

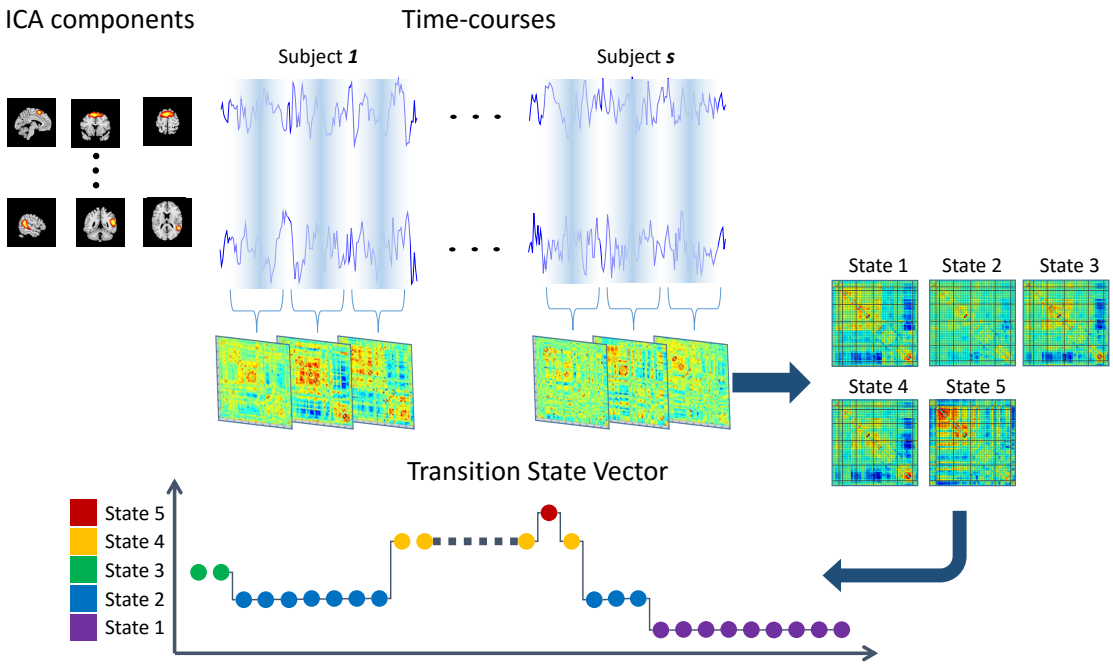

Figure 2.1: Schematic depicting the common procedure for sliding window analysis. A set of dFNCs is computed for each subject on successive sliding windows. FNC in a given window is estimated by calculating correlation matrix. Then dFNC matrices are concatenated along the time dimension for all subjects and clustering is used on the concatenated structure for find recurring patterns of connectivity in the form of connectivity states.

may have distinct frequency profile, frequency-dependent connectivity has also been explored to study how such frequency variation in sources of activities is projected into the synchronicity of the activities.

Spectral analysis of BOLD signal has been proved to help separate noise from neurophysiological sources of signals as well as to identify interesting differences within components of interest. As an example, all used the ratio of low-frequency power to high frequency power of ICA time courses to separate components contaminated by noise from meaningful resting state networks (RSNs). It is also shown that frequency contribution to BOLD signal power spectra varies based on spatial anatomical

structures[32], consistent with other studies [33, 34, 35]. Frequency differences between disease groups in components like the default mode network and others have also been identified [36, 37]. Some other studies have analyzed spectral properties of correlation by estimating coherence which estimates correlation as a function of frequency. For example, in [38] it was suggested that by identifying frequencies contributing to observed correlation we can identify correlation due to respiratory and cardiac activity (which occurs around 0.1-0.5 Hz and 0.6-1.2 Hz, respectively) to provide a better estimate of correlation between auditory/visual/sensorimotor regions which tends to have a lower frequency (< 0.1 Hz) in coherence.

Given dynamic nature of Resting-state connectivity, coherence can be extended to study of temporal dynamics using time-frequency analysis such as short time Fourier transform (STFT), continuous wavelet transform or Empirical Mode Decomposition (EMD). These methods have been applied on many EEG and MEG datasets [39, 40, 41] and to a smaller extent on fMRI datasets [42]. In [43] time-frequency analysis of coherence of EEG rest data is used to find the 7 most stable connectivity networks in time-frequency domain using PCA. [44] used wavelet transform of surface electromyogram (EMG) signal to study dynamic change in power of EMG for their task-based study and [45] used time-frequency coherence between motor cortex and spinal cord to study how it is affected by their designed reaction-time task. For fMRI data, in a relevant study, [1] used wavelet transform coherence (WTC) to show that coherence between default mode (DM) and task positive regions is considerably modulated in the time-frequency domain (frequency-wise the result is consistent with [38]). All these studies suggest that brain regions activations and correlations among them are in fact heterogeneous regarding the frequency spectrum while also being temporally dynamic. However there are limitations to each of these studies. For example although EEG/MEG data have the advantage of higher temporal resolution comparing to fMRI, their low spatial resolution limits the applicability of these analysis to study time-frequency coherence of whole brain regions. For example due

to volume conduction artefact, [43] had to remove the real part of the coherence, an issue that is not present with fMRI. On the other hand [1] as a time-frequency analysis of fMRI resting state data, focused on a few selected brain regions using an ROI method and mainly studied differences in the dynamic nature of positive (in-phase) and negative (out-of-phase) coherence.

In this work we are interested in a whole brain analysis of the above properties. We chose ICA to identify all functional networks of brain in the form of ICA components reflecting the within network connectivity with strong correlation. Our work is built on top of the general framework of studying dynamics of brain connectivity during rest proposed by [26] which has also been used to study patient groups such as bipolar and schizophrenia patients [46, 47]. In [31], similar to ours, is based on spatial ICA decomposition of resting state data followed by sliding-window analysis but here we replace sliding-window analysis with a complex wavelet transform to be able to study FNCs in both time and frequency domain. The wavelet transform is a popular method for time-frequency analysis. The kernel of the transform, referred to as wavelet, is adapted to each frequency so that time-frequency representation has higher temporal resolution in relatively higher frequencies. In complex wavelet transform this kernel is complex and is used to estimate both amplitude and phase of signal at each time-frequency point. Similar to [26], k-means clustering was used as a way of summarizing observed FNCs into recurring patterns of connectivity, here in both the time and frequency domain, which has the direct advantage of studying temporal dynamics and frequency and phase profile of each recurring FNCs independently. We observed that some FNCs patterns seem to have a similar connectivity patterns over a broader range of frequencies while others had a narrow frequency profile. Additionally, we observe that separation of states in the time-frequency plane enables us to find significant and interesting gender differences with respect to the occupancy rates of those identified states, which could not be separated using an approach that did not capture both time and frequency.

2.1.1 Materials

The data in this chapter is the first set of the data mentioned in section 1.4.1, constituting 405 all healthy fMRI scans. GIFT implementation of Group-level Spatial ICA was used to estimate 100 functional networks as ICA components from the data. First 120 subject-specific principal components were retained using PCA and concatenated and then 100 group PCs were estimated via second PCA. Infomax ICA was used to make these 100 PCs maximally spatially independent with 10 repetitions in ICASSO. Finally aggregate spatial maps (SMs) were estimated as the modes of components clusters. GICA1 was used to back-reconstruct subject-specific SMs and time courses (TCs). 50 SMs related to physiological, motion and imaging artifacts were identified and removed from estimated set of SMs. The remaining subset of components are identified as intrinsic connectivity networks (ICNs) and have been used throughout the study. These are the components that have peak activations in grey matter and minimum spatial overlap with vascular, ventricular, motion and susceptibility artifacts. Also time courses are dominated by low-frequency fluctuations. Appendix A represents aggregate SMs of identified ICNs. Time courses of remaining SMs underwent post-processing to further reduce effects of noise which include detrending, motion regression and outlier removal.

2.1.2 Frequency analysis of functional network connectivity over time

We start our analysis by first looking at the frequency spectrum of FNC independent of time (temporally-static). This will help us better understand information we gain by analyzing both temporal dynamic and frequency variability of ICA time-courses connectivity through the proposed time-frequency approach. A well-known approach to studying power spectral density of a signal is Welchs method [48], which is based

on averaging of short Fourier transform of weighted segments of the input signal. Coherence between a pair of signals can be easily estimated as follows:

$$C_{xy}(f) = \frac{P_{xy}(f)}{\sqrt{P_{xx}(f))} \times \sqrt{P_{yy}(f)}} \tag{2.4}$$

Where $P_{xx}(f)$ and $P_{yy}(f)$ are power spectral densities of input signals x and y estimated using Welchs method and $P_{xy}(f)$ is the cross spectral densities of x and y estimated by element-wise Complex Conjugate Multiplication of signals spectral densities. Coherence between ICA time courses was calculated using the above Equation over 5 equally spaced frequency bands in the interval [0.01,0.25]. To ensure valid comparisons of coherence across bands we z-scored coherence values based on the mean and standard deviation derived from a null distribution. Separate null-distribution was created from each components pair and frequency band by estimated the coherence between time courses from different subjects.

2.1.3 Joint time and frequency analysis of functional network connectivity

To adapt Equation 2.4 to capture temporal dynamics of coherence we need to modify Welchs method to include temporal dimension in estimation of coherence. First, inherent averaging over all periodogram (Fourier Transform of weighted segments of signal) should be replaced by a local weighting function. Also ideally the size of these periodogram should be dependent on local frequency content of the signal. To estimate low frequency content we need a relatively larger window size than the one to use to estimate higher frequency content. And at the end when estimating time-frequency coherence between pair of signals, smoothing function over time and frequency dimensions should be introduced to avoid bias toward unity coherence. In our framework, we circumvent these issues by using an adaptive window size and

by employing complex Morlet wavelets that have a Gaussian shape in the frequency domain. The complex Morlet wavelet function is defined as $\frac{1}{\sqrt{2\pi}\sigma}e^{2\pi i f_c t}e^{-\frac{t^2}{2\sigma^2}}$, where t is the time, f_c is the center frequency of the Morlet, and σ is the standard deviation of the Gaussian in the frequency domain. We set the standard deviation (σ) to be equal to 4.3 Hz and the Gaussian centers were equally spaced in the range of $0.01 - 0.25$ Hz (0.01, 0.07, 0.13, 0.19, and 0.25 Hz[1] . To accurately study frequency content of input time series a given frequency of f, we must convolve the Morlet function centered at that frequency over time segments that have at least $0.5 \times \frac{l}{f \times T}$ timepoints, where T is the duration of the segment. For parts of convolution that do not span this length of input signal some padding is typically used which would result into contaminating the transformed result with invalid information. To avoid this problem we define a cone of influence which would only include estimations for which padding is not necessary. Figure 2.2 provides a visual summary of this convolution.

In the following we explain steps of our proposed time-frequency analysis in more detail.

2.1.4 "Dynamic coherence" as a measure of dependence in time-frequency domain

One measure of time series dependency in the time-frequency domain is the Cross Wavelet Transform (XWT) [49]. It is element-wise conjugate multiplication between coefficients of each time series in the transformed domain (Equation 2.5).

[1]Note that our choice of wavelet kernels here is different from what is common in wavelet analysis. In typical wavelet analyses, all wavelets are driven from a mother wavelet but at a different scale and time as follows: $\Psi_{s,\tau}(t) = \frac{1}{\sqrt{s}}\Psi(\frac{t-\tau}{s})$ which defines a wavelet Ψ at scale s and time τ from mother wavelet Ψ. Consequently the output would be a Scale $\times$ Time wavelet coefficients. However there is no uniform mapping from scaling to frequency. In fact, in our case, we use Morlet wavelet but instead of changing the scale we change its frequency center which has an explicit interpretation in frequency domain.

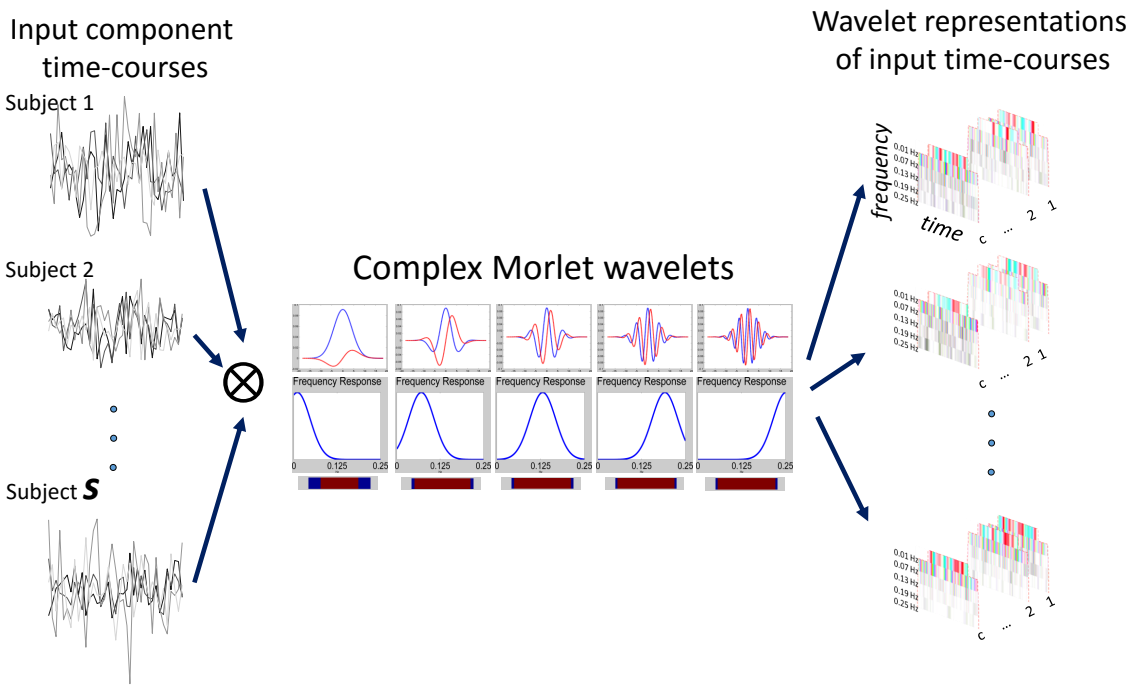

Figure 2.2: Complex Morlet wavelets are used to transform input time courses into the time-frequency domain.

$$W^{xy} = W^{x}. \times W^{y} \tag{2.5}$$

Where W^x and W^y are wavelet transform of input signal x and y and $.\times$ represents element wise conjugate multiplication. The above measure should be normalized by signal spectral power so that coherence estimation is not biased toward parts of the signal with more power. Additionally smoothing function should be introduced on this normalized measure to avoid bias toward unity. This smoothed and normalized measure is called a wavelet coherence transform (WTC) which is defined as follows:

$$R = \frac{S(W^{xy}))}{\sqrt{S'(|W^{x}|^2)}\sqrt{S'(|W^{y}|^2)}} \tag{2.6}$$

Smoothing occurs in both time and frequency and is a function of frequency. This

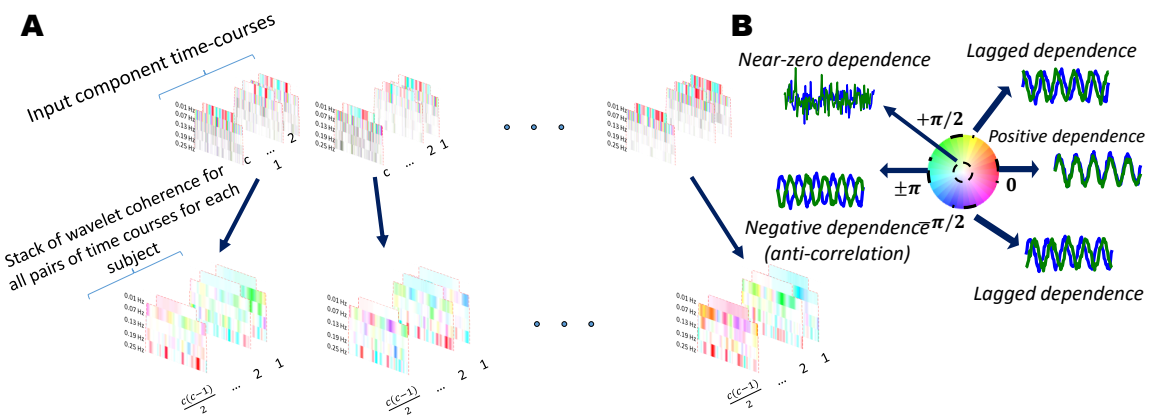

Figure 2.3: Dynamic coherence in the joint time and frequency domain is calculated using Wavelet Transform Coherence between each pair of time-sources, separately for each subject

means that at different frequencies (or scales in the wavelet framework) we have different smoothing radii. Also in a more general form of WTC, the smoothing functions of the numerator and the denominator can be different [50]. We chose the general form of the WTC for our dependency measure and also selected uniform smoothing functions for both numerator and denominator, although weighted smoothing functions can be used as well. We have also adapted smoothing kernel size to the signal properties to maximize true time-frequency coherence estimation which from now on is referred to as "dynamic coherence". In our implementation we looped through sets of possible smoothing parameters on simulated data modeled on the original input data and selected a set of parameters that best capture variation of coherence in time and frequency. More detail is provided in appendix C. Now if we compute the dynamic coherence between all pairs of components of a specific subject at a specific point in a time-frequency domain, we have an estimation of FNC of that subject at that point (Figure 2.3).

2.1.5 Cluster analysis to capture recurring patterns of FNCs in the joint domain

Based on the assumption that some connectivity patterns reoccur in time, here we extend the assumption to the frequency domain and search for FNC patterns that reoccur both time and frequency. To achieve this, we concatenated estimated FNCs along subject-time-frequency (Figure 2.4) and ran a k-means clustering algorithm to find a finite set of k recurring FNCs. For clustering analysis we set desired number of clusters equal to 5. Since our data is large and initial random assignment of the point to random selected clusters may bias the final clusters, we ran k-means 500 times on the same data with random initial guess of clusters assignment and we picked the clustering result which had the minimum sum of distances of each point to its corresponding cluster centroid. Although number of clusters is fixed here, in an additional analysis, we ran k-means clustering with different number of clusters in the range of 2-9 and we observed that cluster centroids in lower model order is reasonably consistent with the ones in higher model order. Also estimation of the F-ratio with different number of clusters confirm our choice of k=5 (more details shown in appendix D). In a separate analysis, we ran k-means separately at each frequency bands using same number of clusters. By using Sammons non-linear mapping and projecting all the captured cluster centroids into a 2-d plane we observed that our original all-band k-means reasonably covers space which is spanned by clusters from each band (more details in appendix E).

2.2 Results

Our results include time-averaged multiband FNCs estimated by Welchs method (Figure 2.5) and repetitive FNCs estimated as cluster centroids in time-frequency

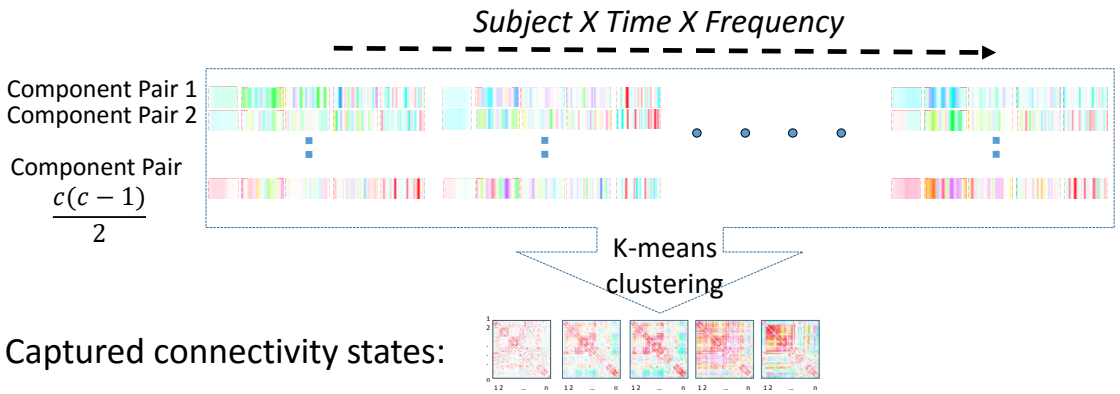

Figure 2.4: K-means clustering is used to find clusters of FNCs along time and frequency dimension for all subjects.

plane (Figure 3). Both types of FNCs are complex values having time lagged coherence encoded in phase. Phase information is encoded with our selected circular colormap and amplitude is encoded as the lightness of the colors (lighter indicates smaller amplitude, Figure 2.3 B). In Figure 2.5 we represent the average of band specific FNCs estimated using Welchs method over all subjects. For each frequency band, we show the average phase of coherence (indicated by color hue) and average strength of coherence (indicated by color saturation) between each pair of components. We also display a polar histogram, indicating distribution of the average phases for all pairs in the matrix.

By close inspection of band specific FNCs we conclude that some component pair time courses have narrow band coherence. Specifically coherence between some Somatomotor and Visual components in second FNC of Figure 2.5 tend to appear in frequencies around 0.07 Hz and attenuate in relatively lower and higher frequencies. The same situation is also true between cerebellar component time courses and many other component time courses. Also we can observe that the coherence phase of those component time courses is a function of frequency. For example, the cerebellar component time courses tend to be either positively or negatively correlated

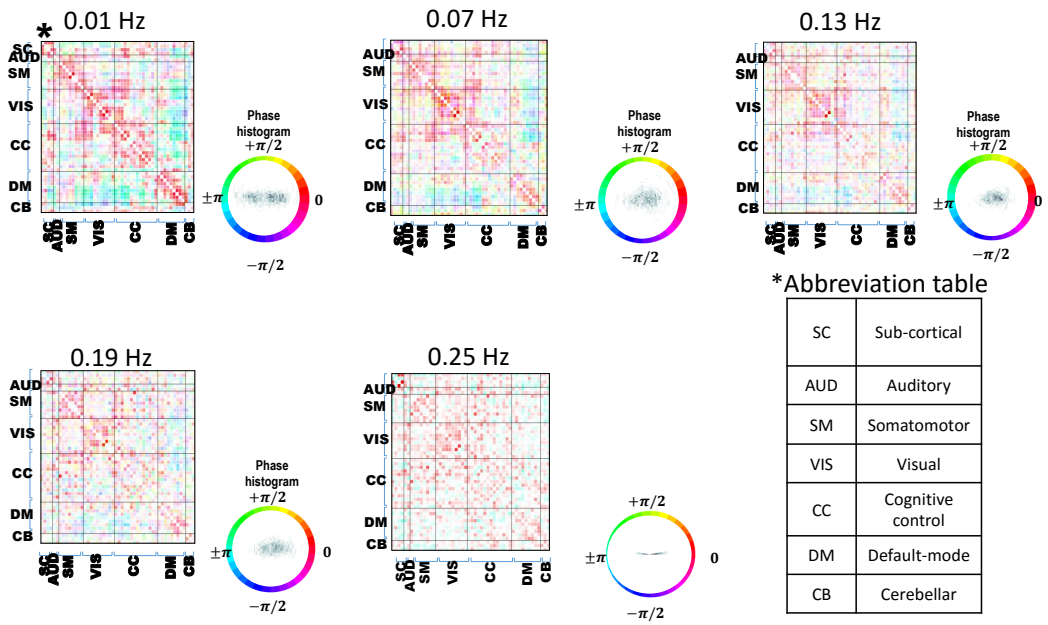

Figure 2.5: Connectivity patterns between components associated with each selected frequency bands integrated over time. As clearly visible, less connectivity structure can be observed in relatively higher frequencies. However due to the integration over time the source of this lack of structure is not obvious in this analysis. Please refer to appendix A for a full display of each component.

to some other components in frequency range of (∼0.01 Hz) and (∼0.15 Hz) but would get lagged (having phase $\sim +\frac{\pi}{2}$) and more uniform in middle range (∼0.07 Hz). It can also be observed that connectivity patterns of Figure 2 tend to have less visible structure in relatively higher range frequencies (∼0.15 Hz). As mentioned in the methods section, because of the averaging in time in Welchs method, it is unclear if this lack of structure in that frequency range is due to low SNR or because of temporal dynamics nature of connectivity. The proposed time-frequency analysis allows us to investigate both frequency content and temporal behavior of the clusters. In Figure 2.6 we represent cluster centroids as the estimated recurring functional connectivity states. States are sorted based on associated rates of recurrence [2]. For each

[2]Since at each frequency band we a different size of cone of interest, we must correct

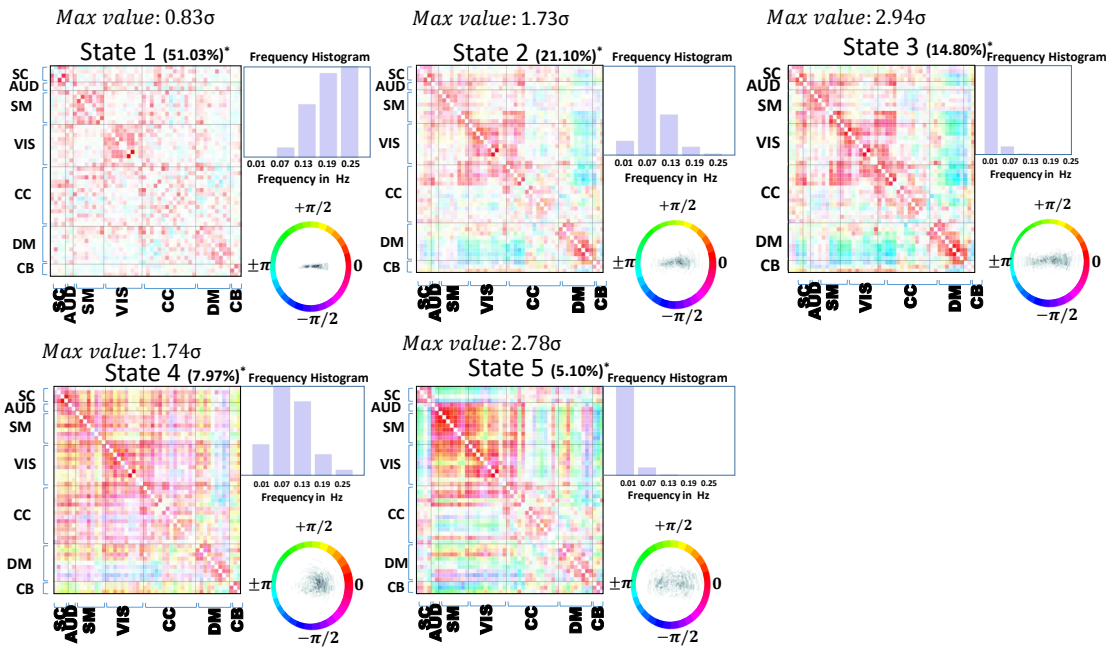

Figure 2.6: Repetitive patterns of connectivity estimated as the cluster centroids formed in time-frequency domain. These patterns (States) are sorted based on their occurrence rates and for each pattern, frequency and phase histogram is presented.

state we have a frequency histogram which shows at which range of frequencies a given state tends to occur. We also include a polar histogram indicating the distribution of dynamic coherence phases across all component pairs and frequencies. This plot represents the degree of time-lagged dynamic coherence between components of each state. State 1 accounts for more than half of the observed FNCs which tend to appear in frequency range of (∼0.15 Hz) and have less phase variation. Relatively strong positive dynamic coherence (phase 0) can be seen among somatomotors as well as visual networks. States 3 and 5 are the centroids of the clusters comprising narrow-band FNCs in the range of (0.01 Hz) with visible variation in phase and with total occurrence of about 20%. Strong positive (in-phase) dynamic coherence

for these lengths to accurately count number of recurrence of each state. To do so, we unwarping clustering results for each subject to have a square shape by replicating the initial and terminal elements, as shown in appendix F.

among visual and part of cognitive control networks can be observed in state 3 and in state 5 this modulation expands to cover strong in-phase dynamic coherence between components in visual, motor and auditory areas (sensor-motor systems). In state 5 sensor-motor systems has strong negative/out-of-phase (phase $\pm\pi$) dynamic coherence with subcortical system which is clearly different from the same connectivity observed in state 3.

States 2 and 4, on the other hand, have wider frequency band though centering on mid-range frequency of 0.07 Hz and consequently having higher total occurrence rates than states 3 and 5. Moreover, we can see that although states 2 and 3 are visually similar to one another but since we use both magnitude and phase of dynamic coherence in our distance measure in k-means clustering and since the two states have different phase and amplitude histogram, the two became centroids of two distinct clusters. Second we have been able to recognize distinct cluster centroids even by having similar frequency ranges (State 2 and 4 both belong to frequency range of (0.07 Hz) and State 3 and 5 both belong to relatively lower range frequencies(0.01 Hz)). This is in fact the direct result of having temporal dynamics as a separate dimension in our analysis. State 4 which has a mid-range frequency histogram is extending our observation in the temporal-static and band specific FNC at 0.07 Hz in Figure 2. In state 4 we also recognize mid-range frequency band (0.07 Hz), phase lagged and synchronous dynamic coherence which was observed in second FNC in Figure 2 but also extending the coherence with same properties to other components pairs such as Sub Cortical-Somatomotor and Sub Cortical-Visual along with few other component pairs.

In Figure 2.7 we represent dynamic coherence pattern specific to state 4 between DM (Figure 2.7 A, Right) and CB (Figure 2.7 B, Right) to other selected networks and emphasizing patterns differences regarding the phase and amplitude to same network pairs in State 2 (Figure 2.7 A, Left) and CB (Figure 2.7 B, Left) which

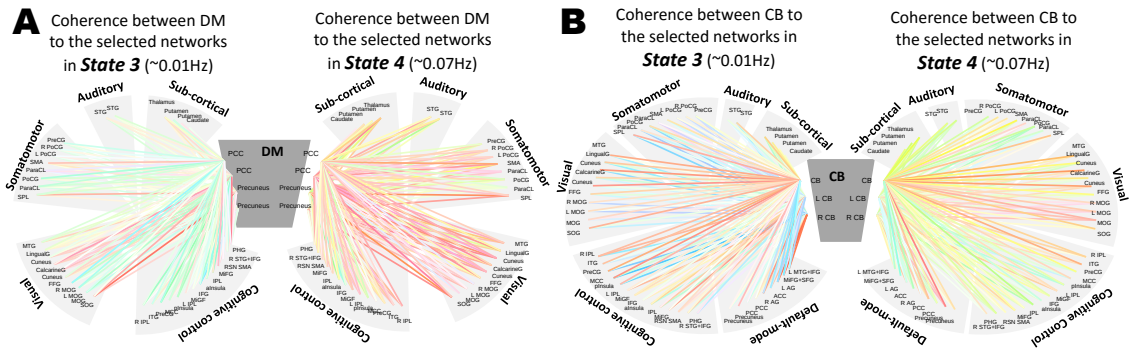

Figure 2.7: In this Figure we emphasize the difference in the nature of coherence based on its phase and amplitude observed in state 3 [Left] (with relatively lower range frequency profile (0.01 Hz)) comparing to state 4 [Right] (with frequency range 0.07 Hz) between (A) Default Mode networks and other selected networks and (B) Cerebellar networks and the rest of the networks

spans relatively lower range of frequencies (0.01 Hz). This unique patterns would have been identified only when we study coherence in time and frequency dimension. Additionally, we investigated gender differences regarding the occupancy of different states. For each subject and for each state we calculated occupancy rate of that state during complete course of the scan. The occupancy measure of a given state is just percentage of time-frequency points that had been labeled with the cluster which is represented by the given state.

After regressing out age and motion parameters in the form of average translation and rotation from estimated occupancy rate, we performed a non-parametric Wilcoxon rank-sum test to compare occupancy rates between males and females. Uncorrected two-tailed p-values were 0.0004, 0.0129 , 0.6672, 0.2895 and 0.3444 for states 1 to 5, respectively, providing strong evidence that males spent significantly more time in state 1 than females (mean $\pm$ SD: 49.5 $\pm$ 5.9% vs 47.4 $\pm$ 7.2%). There is also some weak evidence that females spent more time in state 2 (23.2 $\pm$ 9.6% vs 21.1 $\pm$ 8.0% in males).

2.3 Discussions

In this work we investigated time-frequency sub-spaces spanned by the dynamic coherence among brain regions by first projecting the a measure of dependence into the time and frequency domain using WTC and then, by identifying clusters that dynamic coherence forms in the time-frequency domain using k-means clustering. [1], showed that the nature of the dependence between default mode network (DMN) and the task positive network (TPN) is in fact temporally dynamic yet frequency specific. Consequently we expected to observe similar properties in statistical summaries (cluster centroids) of time-frequency varying measurements of whole brain connectivity. For example states 2 and 3 in Figure 2.6 have similar connectivity patterns and span frequency ranges of (0.01 Hz) and (0.15 Hz) respectively while state 4 and 5 have a narrower frequency profile and unique connectivity patterns. In another aspect of this work, we observed significant difference between males and females in occupancy rates of the two most heavily occupied states. Interestingly, this was only possible because the states were separated along both time and frequency domain. Otherwise the overlap along either dimension would have obscured such an observation. Moreover the complex nature of the chosen kernels enabled us to observe lagged coherence between input signals over the full range, from complete in-phase (0) coherence to complete out-of-phase ($\pm\pi$). Thus, clusters not only differ in the network coherence patterns they present and in underlying frequency content, but phase profiles also play an important roles in cluster formation. Common measure of correlation such as Pearson correlation and mutual information are unable to provide this level of resolution on phase-lagged coherence, although a sliding correlation windows lags (by shifting one time series relative to the other) [51] have been suggested as a correlation-based approach to improving this resolution. Our results encompass a comprehensive set of functional components, obtained from the data using group spatial ICA. With our general framework it is still possible identify

regions among ICA components corresponding to ROIs selected by [1] but we have to keep in mind that [1] chose the wavelet scale as the representation of frequency in their time-frequency analysis of coherence. Scale is one of the parameters that is commonly used in wavelet analysis, which as with short-time or windowed Fourier analysis captures the rate of change of an input signal at a given time (or at a given translation of the wavelet kernel) window. However, the frequency bands of wavelets at each scale do not necessarily have same properties (e.g. usually they have different band widths) which makes it non-trivial to map scale to frequency. Another difference of our time-frequency analysis from the one used by [1] is that in our work the null-distribution has been derived from input data in contrast to the null-distribution estimated through Monte Carlo simulation employed by [1]. Finally we utilized a more general formulation of dynamic coherence as in Equation 3 and discovered through simulation that all of these choices resulted in a better performance that the one used by Chang with respect to sensitivity and specificity measures. More details on the simulation and performance comparison can be found in appendix C. This work can also be seen as an extension of [31] in which repetitive patterns of connectivity were identified along the time dimension. However [31] are unable to capture either the frequency profiles or lagged correlations associated to their recurring FNCs, while here we capture both properties. Comparing the accuracy of estimation of true dynamic coherence in each of these works warrants a bit more explanation. In one scenario, if true dynamic coherence encompasses a broad range of frequencies, then the reliability of dynamic coherence estimates could be diminished by band-limiting the input signal. In this situation, a method more like the one used in [31] would produce a better estimate of true dynamic coherence. However if the true dynamic coherence occurs in a narrower range of the observable frequencies, then band-limiting the input signal before estimating dynamic coherence, as we do in this work, would generally improve estimation accuracy. Additional studies however are needed to more thoroughly understand existing and possible formulations of

dynamic coherence with respect for example, to the kernel and smoothing functions, and to improve the reliability of estimated dynamic coherence.

Chapter 3

Dynamic coherence to reveal novel patterns of RS-connectivity in schizophrenia patients and healthy controls

Functional connectivity of the resting-state brain has been an appealing approach for studying diseases with known brain dysconnectivity aspects such as schizophrenia and bipolar disorders.

Schizophrenia as a complex psychiatric illness has been subject of intensive study. Recent estimates([52]) shows the occurrence rate of 1% of the global population. The main objective of many early studies of this disorder had been the definition of the disorder and diagnosis via symptoms and later moving toward nosology based on evidence rather than nosology merely based on evaluation of the external symptoms [53]. Although there is additional complexity emerging regarding the validity of current state of nosology of disorders [54, 55] we cannot ignore the power of neurobiological

markers such as genetic markers and brain functional and structural maps to help refine the diagnosis. Functional magnetic resonance imaging (fMRI) as a non-invasive method to capture hemodynamic mediated activity of brain regions due to the function of the brain at the given time, is an appealing tool for studying schizophrenia which is thought to be a brain disorder including disturbances of thought, cognition and emotion [56, 57]. Functional connectivity with fMRI has been widely used to study schizophrenia [37, 36] and its popularity comes from the fact that the disease is recognized as a dysconnectivity disorder [58, 59, 60] Evidence of anomalies in brain connectivity of patients goes back at least to early studies [61] in which psychosis was associated with disruption of association fiber tracts in the brain. Since then, extensive work in identifying changes in structural and functional connectivity has been performed. However, structural analysis is unable to capture current functional state of the brain and consequently does not reflect the underlying function of the brain at the time. On the other hand, analysis of fMRI data and observing the activation level of different regions of the brain as well as synchronization of these activations, enables us to study the state of the brain during the performance of an explicit task or during rest. Moreover a degree of consistency has been observed between functional and anatomical abnormal connectivity of the brain[62] which has made the study of both structural and functional appealing to study the disease. Functional connectivity during the resting-state has become a popular and widely used setting in clinical brain studies. Compared to task-based designs, it has been shown that neurophysiological activation during rest spans a broader range of frequencies [15] as well as engaging more functional networks during the course of the scan which potentially provides a more thorough evaluation of functional connectivity comparing to task-based studies [46, 63]. Multiple networks have been identified including the default mode (DM) network which has been associated with self-reflection and self-monitoring [64]. Other networks also have been related to auditory hallucination and paranoid ideation [65]. Resting-state studies of schizophenia include region

of interest (ROI) studies and whole-brain connectivity analysis [66, 67, 68]. General trends is observed dysconnectivity between various resting-state networks. This include observation of hypo-connectivity between wide range of ROIs and also hyper-connectivity among specific regions such as in-between default mode networks and also both inceased and decreased anti-correlation between task-positive and default mode networks [69] using resting-state fMRI)

More recently, dynamic connectivity analysis has been extended to the study of schizophrenia in the context of transient states of connectivity [46] which has extended the observation of static hypo-connectivity in schizophrenia to spending more time in a hypo-connected state. Such analysis has also been shown to be useful in classification process of diseased and healthy subjects [47]. In another group of recent studies, it was shown that evaluation of frequency specific activation enables us to capture significant differences between groups of patients and healthy controls [36, 70, 71, 72]. For example, the default mode network has been shown to exhibit significantly more high frequency fluctuations in patients and significantly less low frequency fluctuations in controls, perhaps related to decreased cognitive efficiency [37]. All of this motivated us to study healthy versus diseased connectivity based on dynamic coherence as it enables us to simultaneously capture temporal behavior as well as frequency and phase profiles associated with each state. In this work we investigated joint characterization of the temporal dynamic behavior of connectivity as well as its frequency and phase (representing lagged dependence) specificity in healthy controls and schizophrenia patients. We show that such decomposition enables us to observe significantly different characterization of connectivity between the two groups. We also observe that when transient connectivity states are defined at the group level and shared among both groups, patients have significantly different tendency toward specific states during the course of the scan than healthy controls as reflected in the dwell time and occupancy rate of each subject.

3.1 Materials and method

We used second set of the data as noted in section 1.4.1. It constitutes of 163 healthy controls with average age of 36.9 and 151 patients diagnosed with schizophrenia with average age of 37.8.

We study connectivity between anatomically and functionally meaningful regions in the brain. Similar to chapter 2, we choose gsICA as the data-driven approach to define these regions with no need for prior knowledge of the regions or a task-design. We used same implementation of gsICA as in section 2.1.1 from which 47 components were selected as the intrinsic functional networks (ICN) subsequently referred to as brain networks. This is followed by a spatio-temporal back-reconstruction step [12] to estimate subject-level spatial maps and time-courses.

Following procedure to estimate connectivity states in joint time and frequency domains (chapter 2), estimations of dynamic coherence for all pairs of networks are concatenated along time, frequency and subjects followed by a clustering analysis which summarizes estimation of dynamic coherence at each point in time and frequency and along each subject into finite number of states represented by centroids of the clusters. Clustering is performed once separately for patients and healthy controls and another time all the subjects regardless of the diagnosis each gives unique perspective on the underlying nature of connectivity states of diseased and healthy subjects.

3.2 Results

The results in the chapter are organized into two sets. In the first set, we estimate connectivity states in the time-frequency domain separately for healthy controls and patients. This allows us to visually inspect differences in connectivity states between

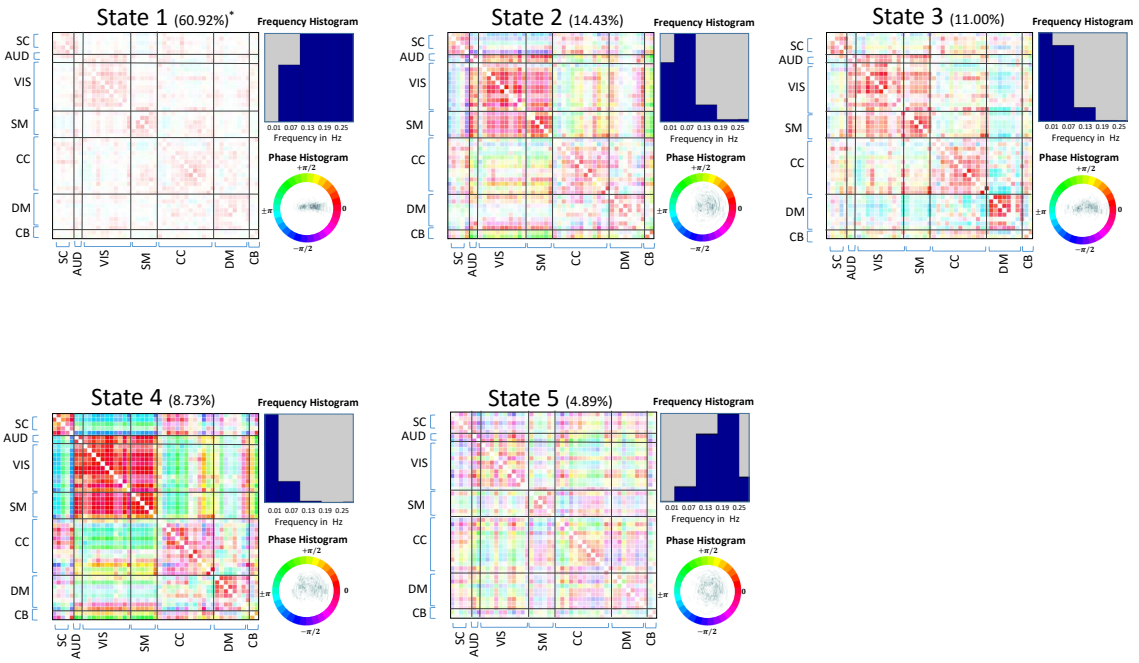

Figure 3.1: Connectivity states of healthy controls defined in time-frequency domain.

patients and controls with respect to their connectivity patterns and their frequency and phase profiles. In the second set of the results we estimate group-level connectivity states, shared among all subjects. This allows us to investigate differences between the two groups with respect to their occupancy rates (amount of time subjects live at a specific state during the course of the scan) at each state as well as their tendency to stay in each state and as we explain, we observed significant differences between healthy controls and schizophrenia patients based on such measures. In Figures 3.1 and 3.2 we show connectivity states as the repetitive patterns of connectivity in time-frequency domain for healthy controls and schizophrenia patient respectively. As explained earlier, phase and frequency profiles of connectivity patterns are also attached to each state along the spatial pattern.

The states for each group of subjects are sorted based on their occurrence rates during the course of the scan. By looking at the correlation between connectivity

patterns of each pair of states belonging to a different group of subjects, as well as visual inspection of connectivity patterns, we can clearly observe that the most commonly occurring state (state 1) is shared among the two groups of subjects and has a high frequency range (frequency profiles are right skewed to the maximum possible frequency of 0.25 Hz). State 3 in HCs has maximum correlation (r = 0.8856) with state 2 in SZs with similarity in both connectivity patterns and frequency profiles. Similarly, connectivity patterns of state 4 in SZs maps to both states 2 and 4 (r = 0.7971, 0.9038 respectively) in HCs however frequency profile of state 4 in SZs only matches frequency profile of state 4 in HCs (Figure 3.2 B). Furthermore, State 3 of SZ and state 5 of HC, although have similar frequency profiles, both have unique connectivity patterns which are minimally any other states of each group . Note that many of these states are only identifiable in the join time-frequency domain. If temporally dynamic states were estimate over all the frequencies [46, 31], any states with overlapping frequency profiles would have been merged and the patterns would have been blurred across states. For example, states 1 and 3 of SZs each has a unique connectivity patterns, specifically a pronounced anti-correlation between somatomotor and visual/auditory/sub-cortical networks in state 3. However given a large overlap between frequency profiles of these two states, dynamic connectivity analyses as have been studied before, would have been unable to capture such unique connectivity pattern as the two states would have been merged across frequency. Next, we identify pairs of components whose dependence is represented by connectivity states that are maximally correlated between HCs and SZs, but exhibit significantly difference in either amplitude or phase of the dynamic coherence due to the diagnosis. Note that since here, connectivity states are estimated from two different group of subjects, we expect observing significant differences in dynamic coherence of between majority of component pairs of each state, but with this analysis we are more interested in directionality of such differences between the groups. As we will explain later, this analysis enables to observe hyper and hypo connectivity differences in

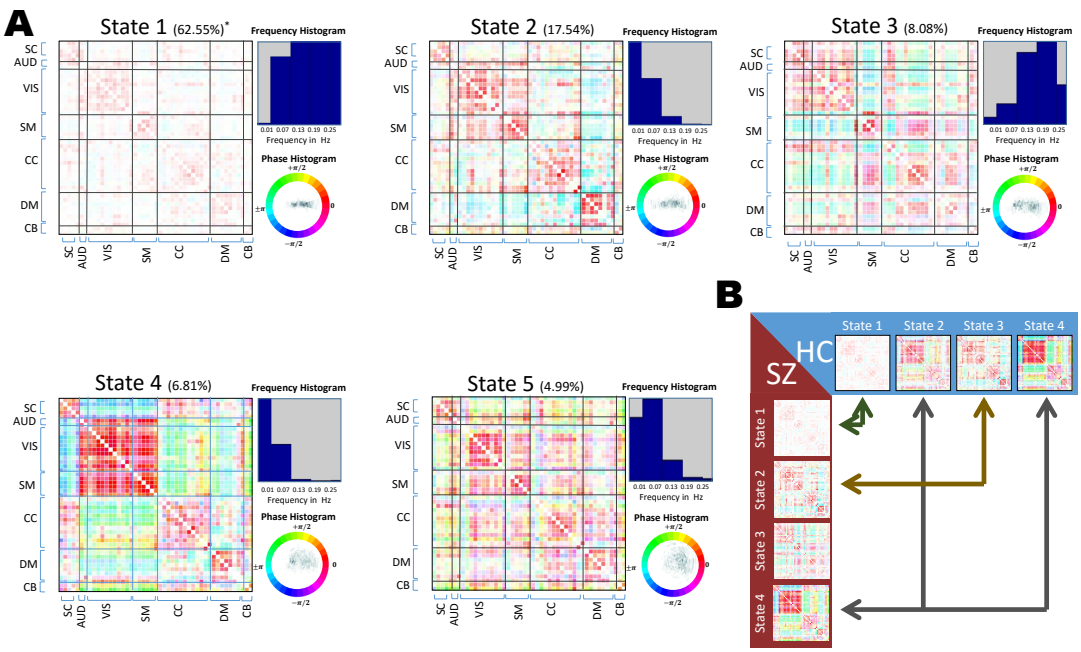

Figure 3.2: (A) Connectivity states of schizophrenia patients defined in time-frequency domain. (B) Maximally correlated connectivity states between SZs and HCs.

maximally correlated states between the groups. For this analysis, for each pair of components and each pair of corresponding states we first derive the distributions of both phase and amplitude of dynamic coherence from subjects in each group. Second, we separately test the null hypothesis that median of these distributions are the same between the both groups of the subjects. The estimated p-values are corrected for multiple comparisons by Bonferroni correction method and the significance level is set to 0.01. To remove susceptibility of the dynamic coherence to the motion as well as gender and age of the subjects prior to the above analysis, we regress out variation of amplitude and phase dynamic coherence due to the above explanatory variables by first, finding the best model which describes subject-wise representation of each state by using MANCOVA analysis and backward model selection [46, 13]. The explanatory variables were diagnosis (0: healthy, 1: schizophrenia), age, gender

(0: male, 1: female), site information and average frame-wise displacement of each subject. The response variable was subject-wise mean of each state as multivariate variable. This analysis was performed separately for phase and amplitude of the response variable. The comparisons between the phase and amplitude of the states at component-level were performed only if the diagnosis variable was among the final reduced model proposed by the MANCOVA analysis and only after regressing out effect of other variables in the reduced model. Figure 3.3 summarizes the analysis of group differences with regard to the dynamic coherence measures of individual component pairs between maximally correlated states as had been shown in Figure 3.2 B. The second column represents difference of the amplitude of the dynamic coherence for the component pairs with significant group differences and the third column, similarly, represents difference in the phase of the dynamic coherence for the same pairs of components. We clearly see that both phase and amplitude contribute in the difference between HCs and SZs for given component pairs. The identification of group differences based on the differences in phase (lagged correlation) is a direct advantage of investigation of connectivity jointly in both the frequency temporal domains. Gray entries are the pairs that could not reject the null hypothesis of no significant difference.

In second set of the results, we further investigate differences between groups by studying the occupancy rates and mean dwell times for patients and controls. As explained above, data displayed in Figures 2 and 3, enabled us to investigate differences in connectivity states between patient and control groups. In this set of results however, we use population-level states to analyze how different groups differentially occupy a common set of states. We perform k-means clustering on all the subjects (regardless of the diagnosis) and identify 5 connectivity states that best describe the data. Figure 3.4 shows the 5 group connectivity states, with corresponding phase and frequency profiles. There are evident similarities between these states and the connectivity patterns in Figures 3.1-3.2, but here these states are shared among all

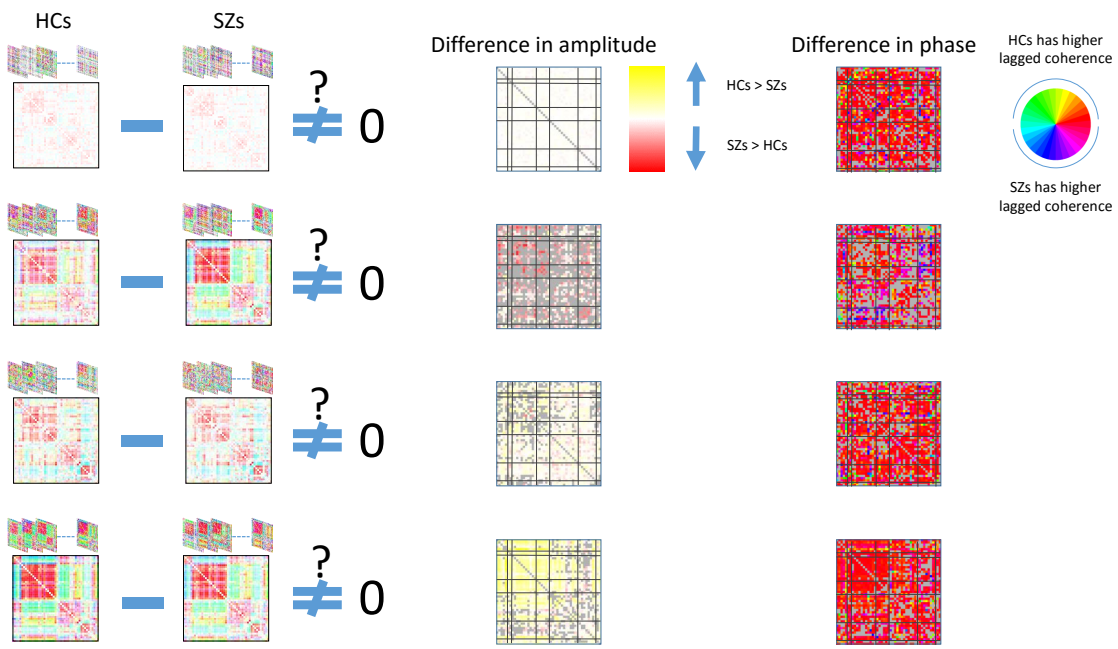

Figure 3.3: Identification of component pairs with significant differences in either amplitude or phase of the dynamic coherence between maximally correlated states. Column 2 shows SZ states which are maximally correlated to the HC states on column 1. Column 3 shows difference in amplitude of component-pair dynamic coherence between HC and SZ which reject the null hypothesis. Gray entries show the ones which did not reject the null. Column 4 shows difference in phase with similar analysis.

the subjects regardless of the diagnosis.

Next, we measure occupancy rates of each subject in each state by counting the number of time-frequency points which were assigned to a given state during the course of the scan. This is followed by group difference analysis on the distribution of dynamic coherence between HCs and SZs subjects and interestingly, in all states except state 4 we observed significant differences between the two groups (Kolmogorov-Smirnov test for difference in medians). Schizophrenia patients were more likely to occupy state 1 (low global coherence, higher frequency profile) and state 2 (negative DMN-to-other coherence, otherwise high global coherence with rel-

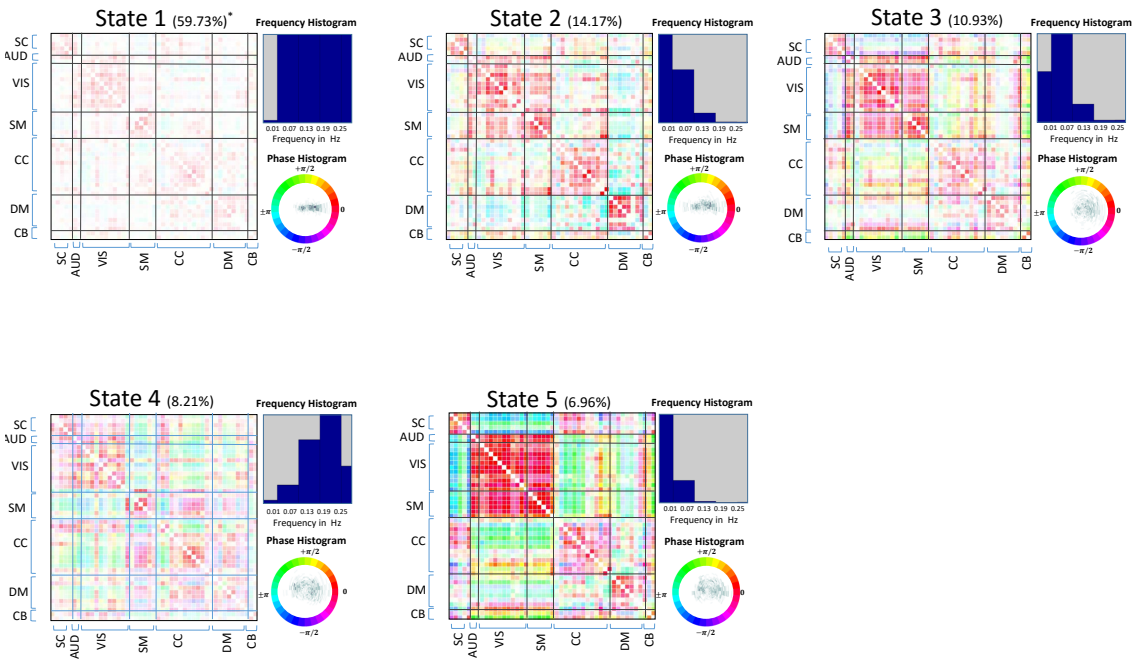

Figure 3.4: Connectivity states defined in time-frequency domain over all subjects regardless of the diagnosis.

atively lower frequency profile). On the other hand, healthy controls had greater tendency to occupy states 3 (high coherence between sensory networks and negative coherence between subcortical and sensory networks and also diminished DMN-to-other coherence with low frequency profile) and 5 (extremely modularized coherence structure, very high intra-domain coherence for all domains plus high subcortical-to-DMN, cognitive control and cerebellum, and very low frequency profile). Group-wise distribution of occupancy rates is represented in column 5 of Figure 3.5.

We also assessed the tendency of subjects toward staying in a given state by counting number of consecutive occurrences of a given state in time which is separately measured for each frequency band. We, then, take the median of these measurements for each subject as our measure of state-specific dwell time. As with the occupancy rate, we find patients have significantly higher dwell-times in states 1 and 2 as rep-

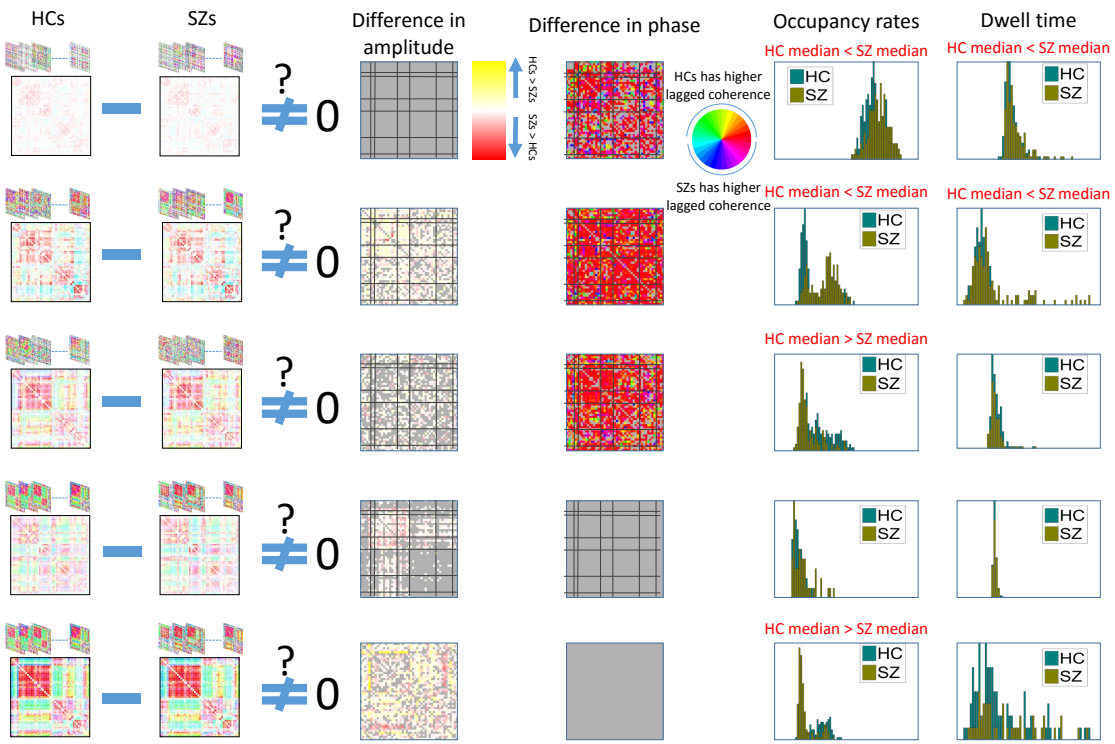

Figure 3.5: Pairs of components with significant difference in either amplitude or phase of dynamic coherence belonging to the same state but in two different diagnosis group. Column 3 represent difference in amplitude and column 4 represent different in the phase of the dynamic coherence. Moreover, column 5, separately, represents histogram of occupancy measure of HCs and SZs subjects and column 6, similarly, represents histogram of dwell times.

resented in column 6 of Figure 3.5. Same as before we regressed out variation due to the other subject-variables (age, gender, site and motion parameters) from both occupancy rate and dwell time measures before conducting these tests. Similar to the results in Figure 3.3 we also identify pairs of components in each state with significantly different dynamic coherence between HCs and SZs. The significance analysis is the same as in Figure 3.3 and the result of the analysis is represented in column 3 (differences in amplitude) and column 4 (difference in phase) of Figure 3.5.

3.3 Discussion

In this study, we investigated time-varying whole-brain resting-state connectivity differences between schizophrenia patients and healthy controls in a framework that smoothly integrates frequency domain characteristics with temporal dynamics of connectivity; phenomena which have been previously explored separately, but not yet combined to allow us to exploit the joint characteristics of dynamic connectivity assessed through the time-frequency domain, providing more informative markers of complex brain disorders When we separately estimated connectivity states of HCs and SZs, we could both identify connectivity states that are shared across the groups as well as connectivity states unique to each group. An interesting observation based on this result is that the most similarity in connectivity between groups is between states with either very high frequency profiles (state 1 of both HCs and SZs) or low frequency profiles (states 2 and 4 of HCs and state 4 of SZs). Consequently, most of the group differences occur in connectivity states with relatively middle range frequencies. It consists of state 5 of HCs with a frequency profile peeking around 0.17 Hz which is minimally correlated to any SZ states and also SZ states 3 and 5 which together cover a range of middle frequencies between 0.07 Hz to 0.17 Hz. There is recognizable modularity in these states which, in fact, makes them unique with respect to the connectivity patterns. For example, in SZ state 2 we clearly observe relatively strong and positive correlation between all the subcortical (SC), auditory (AUD), and visual (VIS) networks. At the same time, somatomotor (SM) networks, different from any other states of both SZs and HCz, are negatively correlated to SC, AUD and VIS networks. To the best of our knowledge, this is the first evidence of existence of such modularity in schizophrenia patients. By taking a closer look at the frequency profile of the state with this modularity, we recognize that, first, this state occurs only in the range of relatively higher frequencies. The most similar modularity among HC states is found in state 5 but with apparent

difference in correlation between SC and AUD/VIS networks which here are anti-correlated rather than being positively correlated as observed in SZ state 2 as well as SM and AUD/VIS with positive correlation compared to the observed negative-correlation in SZs. In previous studies [73, 74] there are reports of hyper-connectivity between thalamus and sensory networks in schizophrenia patients which here appears as a positive connectivity between all subcortical and sensory networks compared to negative connectivity in HCs between same networks. Again we need to emphasize that such observation is only possible when connectivity is studied jointly in the temporal and frequency domains since, first, this modularity occurs in states with a unique frequency profiles (having a mid to high frequency range) and could not be captured when states were estimated over all frequencies, and second, it is different from some other states with which it has an overlapping frequency profile. In fact, if we had studied connectivity only along frequency dimension, states 1 and 2 of SZ would have blurred along temporal domain and we were unable to observe such pronounced modularity unique to SZ. Another observation with this set of results is that the HC states tend to have more dispersion with regard to the phase of dynamic coherence representing lagged dependence rather than positive or negative (anti) correlation. This can be observed from the phase/amplitude histograms of states 2, 4 and 5 of HCs in compare to only states 4 and 5 of SZs with similar dispersion in the corresponding histograms (remember that states are sorted based on their occurrence rates). Based on the observed increased dispersion of phase/amplitude profiles of the HC connectivity states we would expect overall stronger connectivity in HCs compared to SZs. To test this hypothesis, we first, estimate the amplitude distribution of each state as well as the subject-wise occupancy rates of the states and then from these two, we estimate subject-wise amplitude distribution uniformly quantized in 20 bins covering a range of 0 to the maximum amplitude of all states.

Figure 3.6 shows log of the median of these distributions at each bin which is calculated separately for HCs and SZs and we can clearly observe that as amplitude

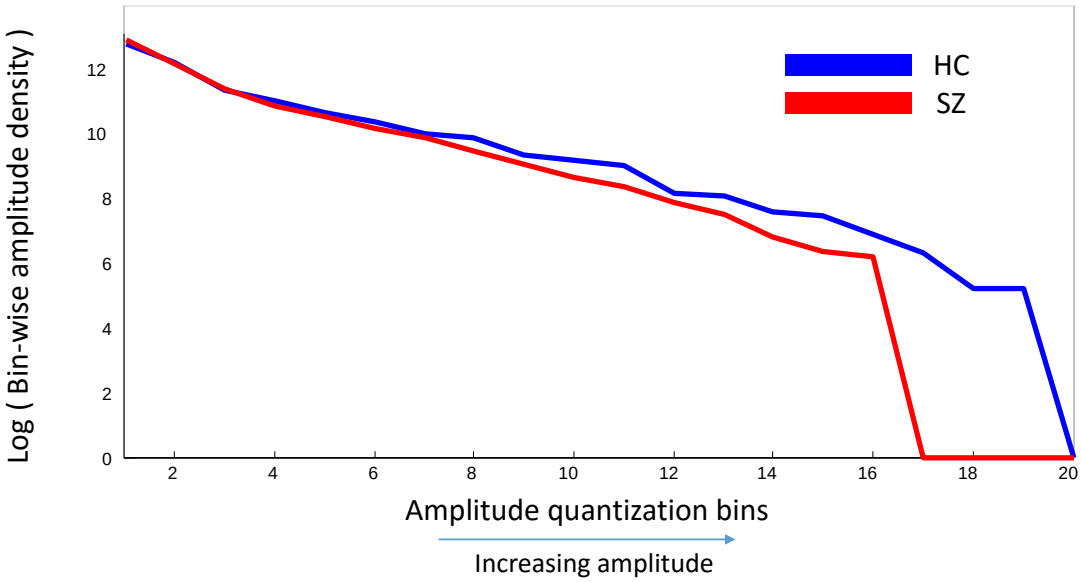

Figure 3.6: Plot showing overall stronger connectivity in HCs compared to SZs.

increases, although log of median of both groups decreases, for SZs, the decreasing rate is much faster. This observation is in line with studies reporting decreased connectivity of SZs between wider range of networks or ROIs [66, 75, 76].

In addition, although HCs showed an overall stronger connectivity than SZs, the dynamic nature of connectivity does not necessarily follow this overall observation. By revisiting rows 2 and 4 of Figure 3, we observe although SZ state 4 has maximum correlation to both states 2 and 4 of HCs, the directionality of the difference in amplitudes changes when SZ state 4 and HC state 2 are compared versus when SZ state 4 and HC state 4 are compared (SZ $>$ HC is color coded as red while HC $>$ SZ is color coded as yellow). This shows that HCs experience both higher and lower amplitude of dynamic coherence in similar connectivity patterns but in different states (2 and 4) in comparison to SZs which have less variation in the amplitude in a similar state and also less frequently (only in state 4). In the second set of the results, similar to study by [46], we investigated group differences in dynamic connectivity in the

form of shared connectivity states between all subjects of both groups. Such analysis allows us to explicitly compare differences in the dynamic behavior of the subjects with respect to occupancy rates of each state by each group as well as tendency to stay in a given state for a period of time (which we refer as the dwell time of subjects in each state). Our analysis shows significant differences between the groups based on both measures which show promise as a foundation for identifying bio-markers to discriminate healthy and diseased individuals. A pronounced observation in this set of result is that, first, SZs have higher occupancy rate and more tendency to stay in state 1 which belongs to high frequency domain. Second, as there is visible contrast between connectivity patterns of states 2 and 3, there are also significant differences between dynamic behaviors of the two groups in the two states. State 2 compared to state 3 has sparser connectivity between sensory networks and also diminished connectivity between subcortical and sensory networks. and also has stronger connectivity (i.e., positive coherence) in-between DM networks as well as pronounced negative coherence between DM and majority of other networks excluding subcortical when compared to state 3. These pronounced differences in the connectivity patterns of the two states are also accompanied by significant difference between dynamic behavior of SZs and HCs as SZs have significantly higher occupancy rate of state 2 than Hs while for state 3 the reverse is true. Moreover, SZ have also significantly higher dwell time in state 2 than HCs. We can interpret this differences as an extension of observed dysconnectivity between similar sets of networks in previous studies [46, 68, 75] to the time-frequency expansion of functional connectivity. Furthermore, similar to the result of the contrast analysis of phase and amplitude of the connectivity states of the first set of the results (Figure 3.3), we observe differences in the amplitude and phase of the connectivities of SZs and HCs which belongs to same state.

Chapter 4

Time-varying spectral powers of resting-state fMRI networks to reveal cross-frequency dependence in dynamic connectivity

So far we have studied dynamic synchronicity among brain regions in the form of connectivity as a function of frequency. This frequency variation of connectivity has sources in frequency variation of activities of the individual brain regions. An aspect which is not explicitly addressed in the proposed approach. Also brain oscillations observed with high temporal resolution modalities, such as magnetoencephalography (MEG) and electroencephalography (EEG), contain spectral power over a wide range of frequencies including theta (4-7 Hz), alpha (7-14 Hz), beta (14-25 Hz) and gamma (low: 30-60 Hz, high: 60-100 Hz).

Moreover, up to now, frequency variation of connectivity had only been studied between same frequency bands and we were unable to capture interaction cross

frequency bands and it is all in spite of the fact that interactions between different frequency bands have been related to higher level functions of the brain such as memory management and cognition [77, 78, 79]. This, in addition to the heterogeneity of brain oscillations across frequencies, has led to the investigation of dependence measures such as coherence [80, 81, 82] and cross-frequency dependence (or, alternatively, cross-frequency coupling (CFC)).

Variations of CFC have been investigated in the form of phase-amplitude coupling, referred as cross-frequency modulation (cfM) [83], phase-phase coupling, referred as phase synchronization [84], and amplitude-amplitude coupling [85]. Particularly, phase-synchronization demonstrated better identification of the underlying cortical connectivity for visual working memory in a combined EEG/MEG study [86]. Further non-linear dependence methods and their applications to EEG/MEG analysis were reviewed in [87] and [88].

Compared to EEG/MEG, the range of detectable frequencies in typical blood oxygenation level dependent (BOLD) fMRI is fairly limited. Recent studies found evidence of frequency variation of BOLD signal interactions however as discussed above, these intersections had only been observed between same frequency bands and there is still no evidence of cross-frequency interactions, though we might suspect the existence of such interactions since the BOLD signal is a correlate of actual brain oscillations as well as underlying brain function.

Here we design a study which enables to observe that: first, frequency content of rs-fMRI networks activity is dynamic in time, and second, that this variation occurs with respect to multiple patterns of spectral powers rather than being specialized to specific sub-bands. These observations led us to the design of a novel metric for measuring CFC in rs-fMRI data. Brain networks, along with their associated time-courses, are captured by independent component analysis (ICA) of fMRI voxel time-series. Estimation of the instantaneous power spectra of network time-courses is

achieved by a time-frequency decomposition. The collection of instantaneous network timecourse spectra are then summarized into a small set of recurring spectral states by applying k-means clustering to time-varying network spectra from all subjects. The cluster centroids define canonical patterns of spectral distributions, which we call Frequency modes. Without making any prior assumption on the properties of these modes, we observe different spectral density shapes emerging naturally from the data while simple band-pass filtering is unable to capture such information.

Taking a step further, we analyze the occurrence rate of each mode in the original network time-courses, as well as the co-occurrence of pairs of modes, which we use to define novel measures of cross-frequency dependence.

Significant gender and age effects are observed with both the occurrence and co-occurrence measures for some specific networks and network pairs, respectively.

We conclude this study by pointing out that although fMRI data suffers from low sampling rate and, being a hemodynamically mediated signal which includes only a narrow range of detectable frequencies, there are detectable dynamics and cross-frequency dependencies in the data which have not been explored before. Significant age and gender associations illustrate the richness in this kind of information.

4.1 Material and method

We used exact same data set as described in section1.4.1 with same pre and post processing as in section 2.1.1 which similarly resulted in decomposition of data into 50 maximally independent components as the representation of brain functional networks and the corresponding subject-wise time-courses (appendix A)

4.1.1 Estimation of Instantaneous Power Spectra of network Time-courses

To capture recurring frequency modes of network time-courses, we use same time-frequency decomposition of network time-courses as in section 2.1.3. The only difference is that here we center each wavelet in 20 uniformly selected frequencies of the interval of 0-0.25 Hz compared to 5 centers as described in section 2.1.3. This would only let us having a better frequency resolution.

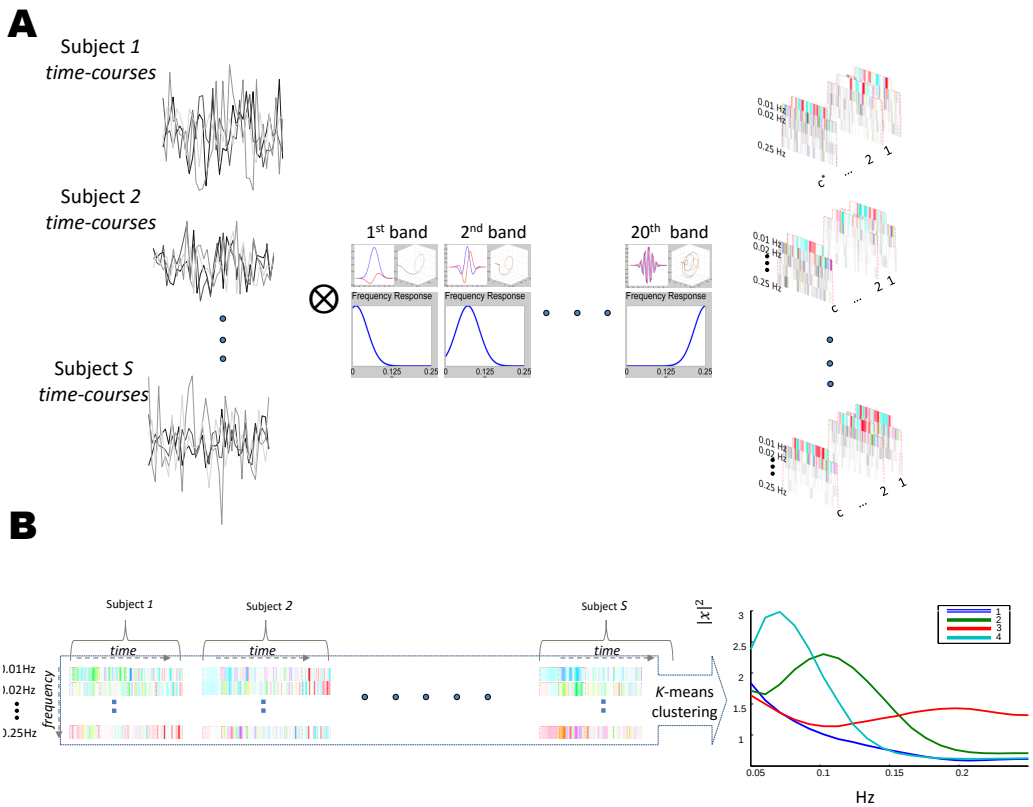

Figure 4.1: Outline of our framework for capturing instantaneous spectra of ICA time-courses in time in the form of frequency modes. (A)Complex morlet wavelet is used to map the time-courses to the time-frequency domain. (B) canonical patterns of power spectra are estimated by k-means clustering which we refer to as frequency modes.

To make our estimation less susceptible to random variation of signal due to noise artefacts, we z-score our estimation of time-frequency decomposition of a given time-course from our estimation of null-distribution. The null-distribution is derived from bootstrap resampling of the same time-course when its time-points are randomly reshuffled to remove any periodic behavior of the signal. This is repeated for 200 times and wavelet decomposition of each of these shuffled time-courses is estimated. By concatenating these decomposition along time, we estimate the null-distribution at each frequency. Concatenation of amplitudes of these z-scored time-frequency decompositions of all network time-courses of all subjects forms a 2-d matrix whose one dimension is frequency power spectral and the other dimension is $time \times network \times subjects$. Given that, clustering of frequency-amplitude dimension along the time dimension would capture dynamic and recurring frequency modes. In this work we used k-means clustering with $k = 4$. Figure 4.1 summarizes all these steps along with the captured frequency modes as the result of the proposed method.

4.2 Results

Frequency modes are, in fact, centroids of clusters that are formed by instantaneous spectral powers of all ICA time-courses. The modes represent short-lived and periodic activities of time-courses. The occurrence rate of these activities forms the corresponding spectral densities as is presented in Figure 4.2 .

Frequency modes, by design, are shared among subjects and networks and F-ratio analysis suggests that 4 of these shared modes explain most of the variations of spectral powers. However, there are different aspects of the modes which may vary between subjects and networks. First, frequency modes vary with respect to the range of frequencies they span. For example, while mode 4 spans a relatively narrow range of frequencies comparing to other modes and its spectral density has positive

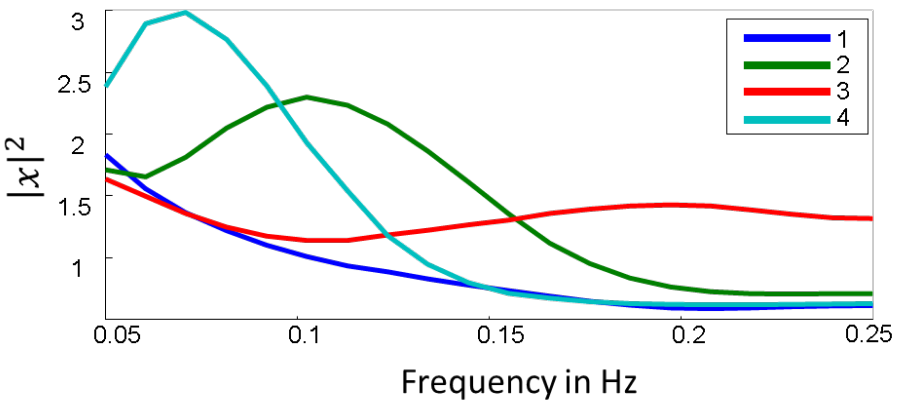

Figure 4.2: "Frequency modes" as the representatives of the variation in spectral powers of networks time-courses, Each mode is formed by similar instantaneous frequency content of time-courses which have been clustered together.

skewness (left-modal), mode 2, on the other hand, spans middle-range of frequencies with the peek around 0.1 Hz and mode 3 has more uniform spectral density along all range of frequencies and with a slight negative skewness (right-modal) and a peek at 0.20 Hz.

Next, we investigate two other aspects of the modes which vary among subjects and networks.

The first aspect is the occurrence rate of individual modes in each of the networks which is measured by counting number of time-points of a given network time-course which has been assigned to a certain mode as the result of clustering (Figure 4.3).

The second aspect of the frequency modes is conditional co-occurrence (***c***co-occurrence) of these modes. As mentioned earlier, since each mode has a unique spectral density, by investigating co-occurrence between each pair of modes, we are in fact exploring a measure of cross-frequency dependence of ICA time courses. Conditional co-occurrence is defined

here as a conditional probability of occurrence of a specific mode (assume mode **i**) in a given network (network **m**) given that another mode (let it be mode **j**) has occurred at the same time-point in another network (network **n**). Mathematically speaking we measure:

$$\begin{aligned} Cco - occurrence\,(\text{modes} : \mathbf{i}, \mathbf{j} \text{ in networks } \mathbf{m}, \mathbf{n}) = \\ \Pr\,(\text{mode } \mathbf{i} \text{ in network } \mathbf{m} \mid \text{mode } \mathbf{j} \text{ in network } \mathbf{n}) \end{aligned} \tag{4.1}$$

The above measure, alone, does not estimate the degree of dependence and we need to compare it against the observed cco-occurrence given that modes $\boldsymbol{i}$ and $\boldsymbol{j}$ occur independently from one another in networks $\boldsymbol{m}$ and $\boldsymbol{n}$ respectively. Based on independence assumption $\Pr\,(\text{mode } \boldsymbol{i} \text{ in network } \boldsymbol{m} \mid \text{mode } \boldsymbol{j} \text{ in network } \boldsymbol{n})$ needs to be equal to $\Pr\,(\text{mode } \boldsymbol{i} \text{ in network } \boldsymbol{m})$ which is simply, the occurrence rate of mode $\boldsymbol{i}$ in network $\boldsymbol{m}$.

Consequently, our reported estimation of cco-occurrence is z-scored estimation of above cco-occurrence measure from estimated distribution of $\Pr\{\text{ mode } \boldsymbol{i} \text{ in network } \boldsymbol{m} \}$ which would serve as our null distribution. Values around zero imply an independence of occurrence of mode i from mode j in the given the networks. Values greater than zero implies positive dependence of mode i on mode j and negative dependence when the value is less than zero. Figure 4.4 represent cco-occurrence of each pair of modes for all networks as a $C \times C$ matrix where C is number of ICA-networks (50 in this study). We call these

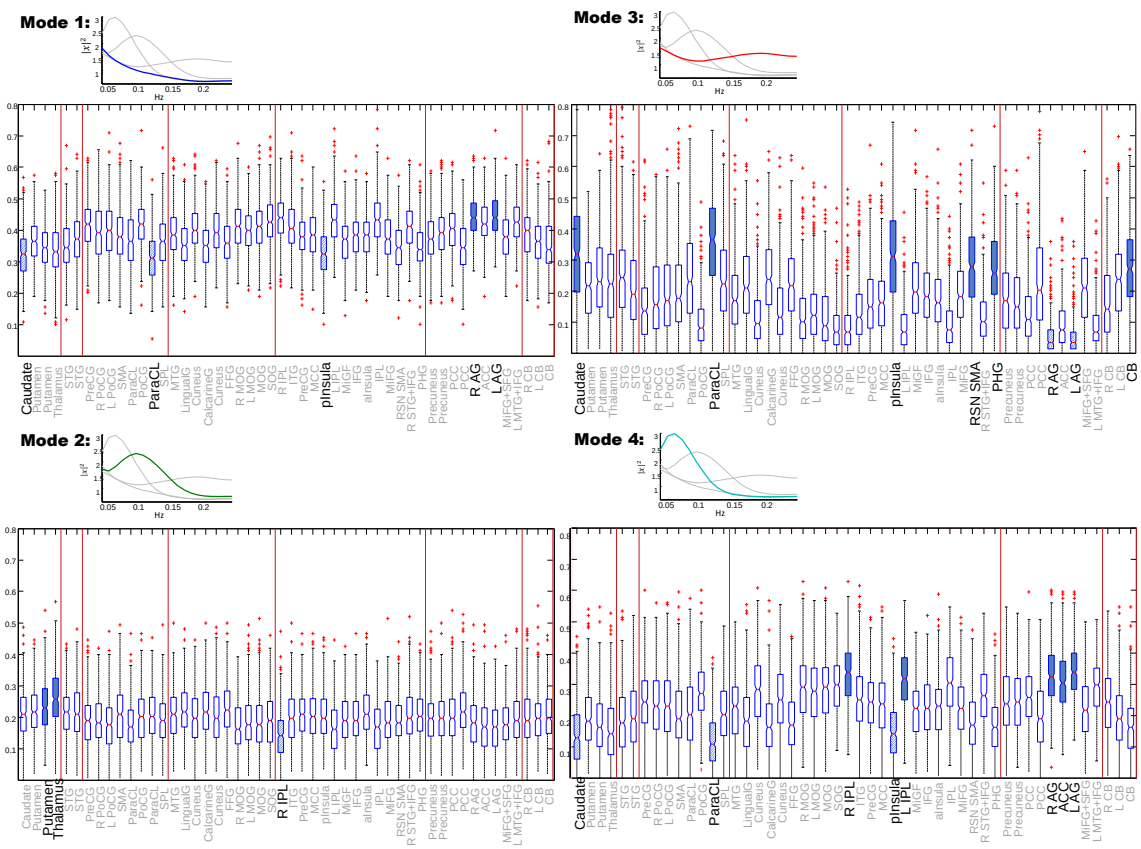

Figure 4.3: Boxplots of occurrence rates of each individual frequency mode in ICA networks. Networks with significantly higher (filled boxplots) or lower (dashed boxplots) occurrence of the given mode than majority (85%) of all networks are identified.

matrices cco-occurrence maps. In the last part of the results, we focus on studying variation of individual occurrence of modes as well as cco-occurrences of pair of modes between networks due to the age and gender of subjects.

Variation in occurrence rate of modes between networks can be investigated by boxplot representation of the rates from all subjects for each network. For each mode we identify networks which have signif-

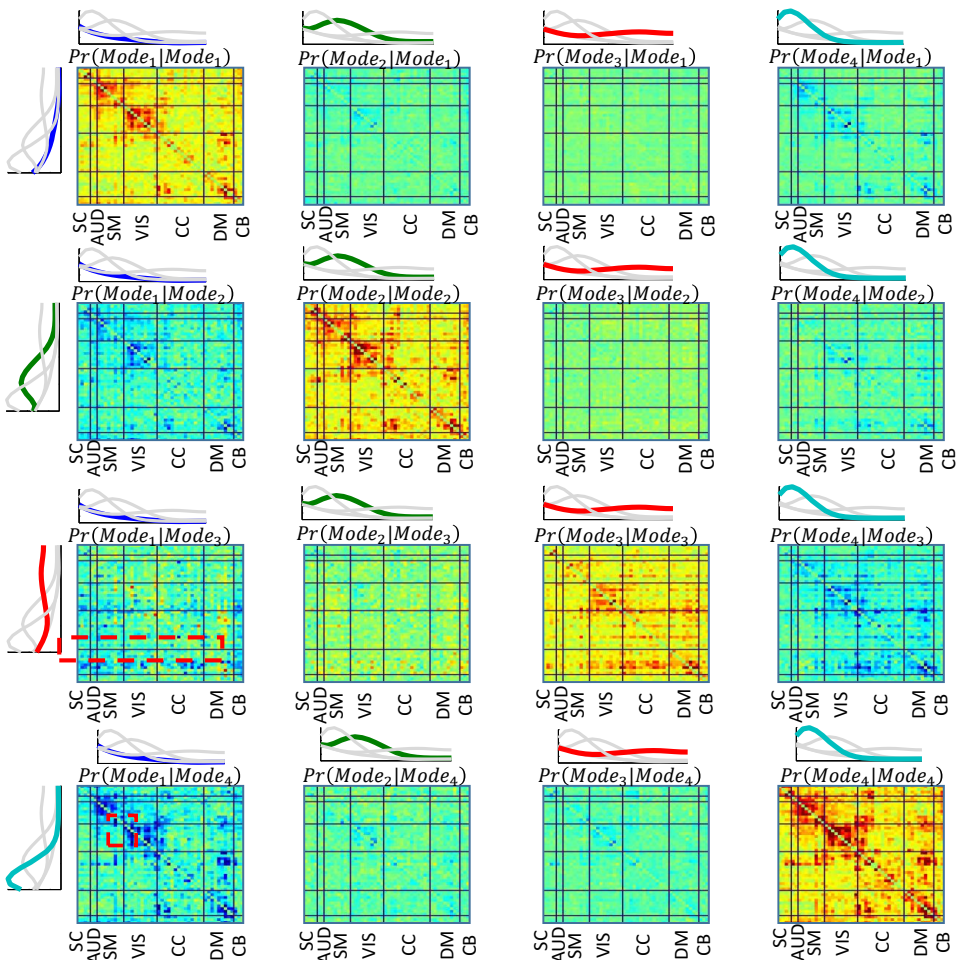

Figure 4.4: Cco-occurrence maps of frequency mode pairs. An entry (column m, row n)(1...50, 1...50) of a matrix at column i (1...4) and row j (1...4) of the Figure shows cco-occurrence of frequency mode i in network m, given that frequency mode j is occurred at the same time-point in network n. Positive cc-occurrence (color coded as red) corresponds to reinforcement effect and negative cc-occurrence (color coded as blue) is corresponding to suppression effect. (SC: Sub-cortical, AUD: Auditory, SM: Somatomotor, VIS: Visual, CC: Cognitive Control, DM: Default-mode, CB: Cerebellar)

icantly higher or lower average occurrence rates than majority of all networks. For this analysis, first, we performed pairwise 2-sample t-test between all network pairs. The estimated p-values were adjusted

to account for the multiple comparisons using the false discovery rate (FDR) approach. Second, we identified networks which had significantly (FDR adjusted p-value < 0.01) higher (solid filled box-plot in Figure 4.3) or lower (dashed box-plot in the same Figure) average occupancy rates than 80% of all networks. We also study the effect of age and gender of subjects on the estimated occurrence rate of modes through a multivariate analysis of covariance by setting the occurrence rate of each mode in all the networks (a 50-d vector for each mode) as the response variable. The design matrix includes age, gender and two motion parameters (average translation and rotation of each subject) as well as pair-wise interactions of these predictors. This followed by a backward selection of the subset of significant predictors. Backward selection implementation of MANCOVAN toolbox was used to perform this procedure. For more details on the multivariate analysis please refer to [13]. The multivariate analysis determines the subset of predictors which significantly affect occurrence rate of each mode over all networks. If the reduced model included either age or gender as significant predictor we can identify individual networks in which given modes occurrence rate is significantly affected by either of those predictors. Univariate analysis for each individual network is used for this part. First, predictor of interest is picked (which is either age or gender if included in the reduced model). Then the effect of other predictors in the model is regressed out from oc-

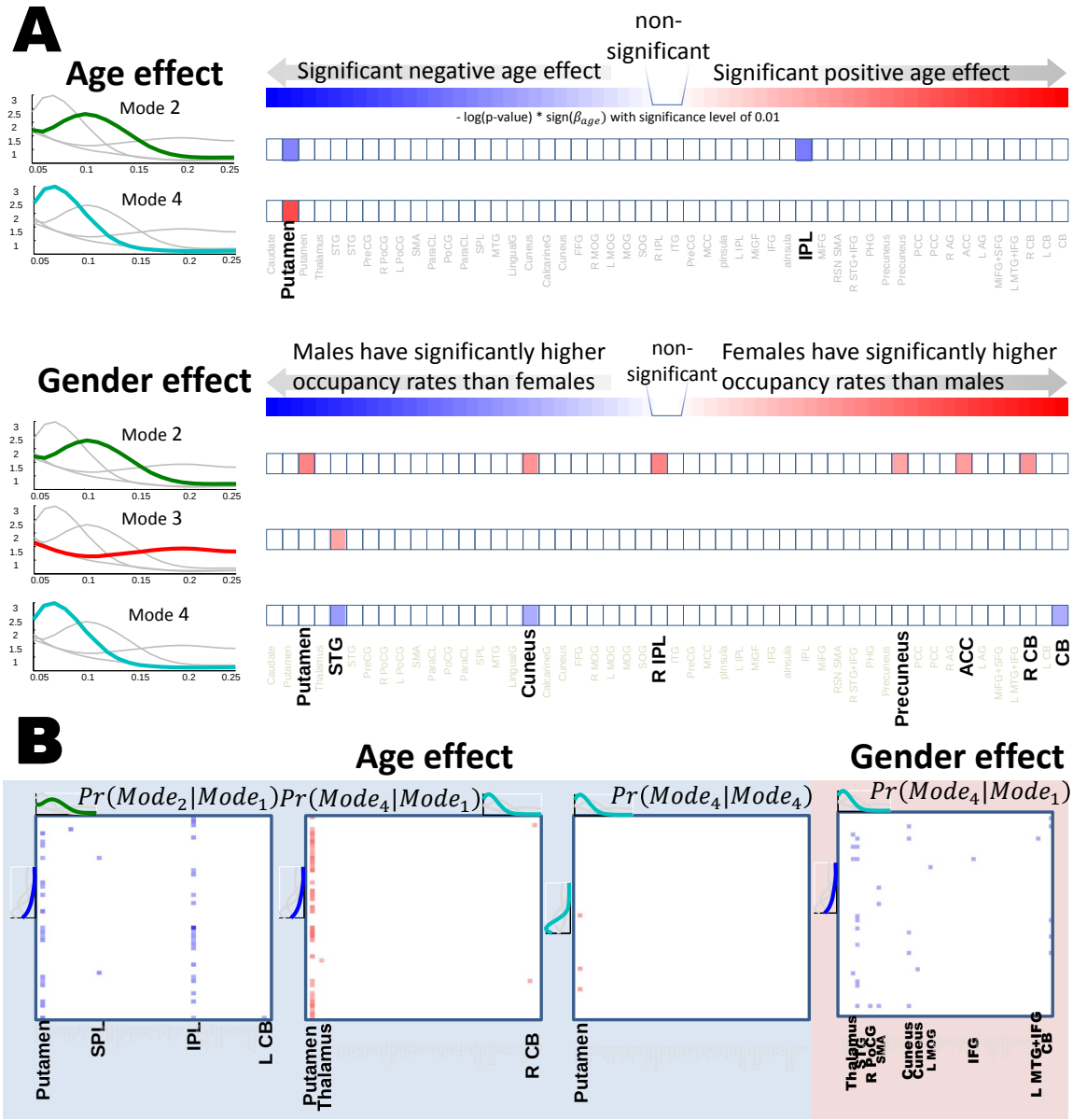

Figure 4.5: Analysis of age and gender effect on **(A)** occurrence rate of individual frequency modes and **(B)** cco-occurrence rate of pair of modes. In **(A)** specific networks and in **(B)** pairs of networks are highlighted (bold) in which occurrence rate of given mode and cco-occurrence of pair of modes are significantly effected by age or gender

currence rate of the given mode in individual networks through a linear regression. Finally, a linear regression is applied between the selected predictor and the residual of the previous regression as the response variable. After running this for all networks, the estimated p-values are FDR adjusted for the multiple comparisons and the ones which survived the significance level of 0.01 are reported. Figure 4.5 A shows $-\log$ (FDR-Adj p-value $\times$ $sign$(regression coefficient) for networks with significant age and gender effect on mode occurrence rate. The sign of the regression coefficient shows direction of influence. For age effect it shows if the measure is increased or decreased by age and for gender, positive coefficient means the measure of interest is higher in females since female is encoded as '1' and male as '0'. A similar analysis can be used to study variation of cco-occurrence of frequency modes between networks and subjects. Each cco-occurrence map, by itself, shows variation among networks. For example, from the maps along diagonal which represent dependence between same modes, we are observing that although there is relatively higher dependence between all networks comparing to the observed dependence in the other maps, dependence within somatomor and visual networks is stronger. To study subject related variation of co-occurrence maps due to age and gender of subjects, we follow similar analysis to the one we used for the occurrence rate of individual modes. The design matrix would stay the same and the response variable would be the cco-occurrence

maps of each pair of modes. Same as before, Figure 4.5 B shows $-\log$ (FDR-Adj p-value $\times$ $sign$(regression coefficient) for pairs of networks in which co-occurrence of given pairs of modes is significantly affected by age and gender. Interpretation on the directionality of the influence and the color maps for p-values stays the same as in Figure 4.5 A.

4.3 Discussion

This study adds to the growing evidence that, although fMRI data has typically been assumed to be frequency invariant (mostly due to its low acquisition sampling rate and consequently narrow range of detectable frequencies), even within that narrow range of frequencies, connectivity varies both within and across frequencies. In this work, by employing frequency modes that capture characteristic spectral power distributions, frequency variation is observed in individual network time-courses. Conditional co-occurrence of these modes is our measure of cross-frequency dependence between brain networks.

There are interesting observations that can be made based on cco-occurrence maps in Figure 4.4. First, positive cco-occurrences observed in diagonal maps which correspond to cco-occurrence of same frequency modes, resembles familiar modularity in resting state func-

tional connectivity including connectivity between Default Mode(DM), Visual (VIS) and Somatomotor (SM) networks. In fact, occurrence of a given mode in each of these networks reinforce occurrence of the same mode in those other networks. We call this effect a reinforcement effect. Continuing with this observation, if there did not exist any dependence across frequency modes we should not have observed any positive (reinforcement) or negative (which we call suppression) cco-occurrence in off-diagonal maps which is obviously not the case. For example, column one represents an interesting suppression effect on Mode 1 by other modes. Mode 1 has lower power at every frequency than any of the other modes, representing very weak signals with spectral power that decays in frequency. Between network-pairs that tend to show high correlation in conventional FNC analyses, the two modes with highest aggregate power (*i.e.* modes 2 and 4) seem to self-reinforce, while both separately suppress the probability of seeing mode 1 with low-magnitude spectrum with decaying frequency. This leads us to conclude that networks with strong signals selectively reinforce networks with similar frequency regime while also suppressing the odds that such a network presents relatively weak signal with decaying frequency. Strong, but spectrally dissimilar (*i.e.* mode 2 and mode 4), signals in characteristically connected network-pairs are relatively indifferent to each other, neither reinforcing nor suppressing the co-occurrence of one and another that would occur under an assumption

of independence.

Note that, by looking at the maps in the row corresponding to a given mode, we can identify modes that are more likely to be either reinforced or suppressed by the mode associated with that row. For example, maps on the second row, represent the effects of conditioning on mode 2 , which has significant overall power focused in the middle range of frequencies. Observing maps along this row we see that well-powered network signals focused in middle-range frequencies reinforce similar regimes in certain other networks, suppress weakly powered signals from these networks and have limited effects on the probability of observing the modestly-powered higher-frequency mode 3 or the strongly-powered lower frequency mode 4.

Additionally, although it is observed that mode 1 is more prone to suppression effect by the other modes, we also observe same effect by mode 3 on mode 4 and this constitutes one of the key observations of the work we are reporting here. By taking a closer look at the power spectrum of the third mode we can easily observe that this mode is middle-powered and represents a wide range of frequencies, peaking slightly at the relatively high frequency (0.20 Hz including frequencies which have been usually associated with non-physiological sources of variations such as motion artefacts that are commonly filtered in BOLD analyses). On the other hand, mode 4 has a spectrum very

similar to that of the BOLD signal, and the map at row 3 and column 4 illustrates an interesting suppression effect on this mode on a subset of networks in VIS, cognitive controls (CC) (including IPL) and DM (including R/L AG and ACC) by thigh mid-powered, higher-frequency mode 3. Commonly held beliefs about the nature of fMRI data would not suggest any dependency between these modes since these two are supposed to belong to very different sources of variation in captured signal [89, 38].

Furthermore, through a regression analysis, we observed that cross-frequency dependence may vary between different group of subjects. Specifically, we observed an age-correlated increase in the suppressive effect of networks in mode 1 on putamen and IPL when in mode 2 and, simultaneously, an age-correlated increase in the reinforcement effect of networks in mode 1 on putamen when in mode 4. This observation is interesting since the putamen is part of the sub-cortical domain of networks which is understood to be broadly connected to cortical networks [90] and these connections are believed to be involved in cognitive functions [91]. Although study of aging brain is out of scope of this work(and the range of subject ages in this study is limited) such an observation highlights the potential benefits of incorporating cross-frequency dependence measures in connectivity-based aging brain studies. We also found that subject gender was associated with

cross-frequency dependence, an interesting observation whose neurophysiological interpretation is also beyond the scope of this work.

Before concluding this section, we need to further clarify the actual nature of the instantaneous activities that each frequency mode is representing. The most important consideration in interpreting frequency modes is that each occurrence of a given mode is in fact representing instantaneous but "periodic" activities which consist of instantaneous activations and de-activations of the signal. The frequency spectrum of each mode represents the occurrence rate of these activations and de-activations. Consequently, a co-occurrence between two modes could be representing either positive or negative correlation since instantaneous activation of one signal could be aligned to either instantaneous activation (*i.e.* positive correlation) or de-activation (*i.e.* anti-correlation) of the other signal. In conclusion, reinforcement and suppression effects should not be associated with the commonly used correlation or anti-correlation measures.

Chapter 5

Conclusion and future works

In chapter 2 we have proposed a novel framework to study time-frequency dynamics of functional connectivity of resting-state fMRI data through a data-driven approach. Spatially independent components have been identified using spatial ICA, then the dynamic aspect of corresponding subject-specific functional network connectivity is studied in both time and frequency domains using wavelet transform coherence. Dynamic coherence of time courses is summarized by a finite number of recurring patterns of connectivity estimated by k-means clustering of the complex-valued FNCs. In this framework each FNC is in fact a snap shot of coherence between all pairs of ICA components at a time-frequency point

An important advantage of this approach is that derived connectivity states are separated along both the time and frequency dimen-

sions meaning connectivity state of the brain at given time-point can be studied as a superposition of multiple frequency-specific connectivity states while still retaining temporal dynamic nature of the states. Additionally, the phase information encoded in the connectivity state frequency information enables us to capture a delayed and temporal dynamic correlation.

Limitations of this work include interpretability of the results and the methodological choice. Regarding the interpretability, this work is predominantly methodological and has been applied here for general illustrative purposes to resting state data. The nature of resting state data make it difficult to determine the true source of whole-brain connectivity patterns arising from different frequency profiles or distributions; it may have roots in physiological properties of spatial maps and differences in their activation, or could even be due to systematic noise during the scan. In terms of interpretability, this work can be easily applied to task-based imaging studies, including those that capture cognitive states or to studies involving prior information on subject cognitive states [92]. It can also be extended to multi-modal frameworks and applied in studies such as [93] , which could result in better neurophysiological interpretations of observed connectivity patterns. Also such work can help identify the relevance of the functional networks contributing to the observed FNCs under various conditions

in order to better understand and interpret identified networks coherence behavior.

As always we are limited by our assumptions, and also methodological choices based on those assumptions. For example, here we have assumeds that FNCs form clusters in the time-frequency domain that can be captured by k-means clustering, a method that looks for clusters with convex boundaries, although more complicated clustering approaches such as spectral clustering have been proposed to capture more general shapes of clusters. Recent studies have also taken advantage of linear decomposition to break down observed FNCs into a finite number of connectivity patterns. For example [29] used PCA to linearly decomposed observed FNCs into finite set of connectivity patterns which are mutually spatially orthogonal and [30] looked for finite set of connectivity patterns that are mutually temporally independent and have linear contribution to the observed FNCs. CAP analysis as one of the more recent techniques to study dynamic connectivity has drawn the community's attention. CAP however, like many other approaches to dynamic connectivity,oapproaches is unable to capture frequency heterogeneity within the temporal dynamics. Future work studies could investigate ways of integrating these decompositions in a broader approach to time-frequency analysis. Lastly, there are many other approaches to studying time-frequency proper-

ties. empirical mode decomposition [94], for example, estimates the instantaneous frequency of a given signal. Based on [95], with correct settings, many time-frequency analyses can be made equivalent, so future studies might investigate the consistency of results across different approaches. Our framework does not limit us in the choice of time-frequency analysis method, so any advances in this area would only strengthen the approach we propose as currently implemented.

In chapter 3, resting-state connectivity of two healthy and diseased populations is studied in a joint domain of time and frequency. The result showed strong evidences on the simultaneous variation of connectivity in both domains and revealed novel differences and similarities between diseased and healthy, unique to the study of connectivity in the join domain and consequently obscured in previous studies of resting-state connectivity of schizophrenia.

In chapter 4 we looked at the dynamic variation of frequency at the activation level and argued that not only the synchronous activity of functional networks varies in time and frequency but also activation of individual networks experience varying frequency profiles referred here as *"frequency modes"*. We further discussed that such analysis enabled us to provide first evidence of cross-frequency dependence in fMRI networks.

As mentioned earlier, one of the major limitations of the proposed

measure of cross-frequency dependence is its inability to estimate directionality of dependence in the way that correlation could measure in the form of positive and negative correlation. However, we believe that by investigating possible approaches to incorporate phase information in a possibly new measure of cross-mode dependence we would be able to measure the directionality as well.

Also this work is introduces a method of capturing richer information about inter-network frequency-dependencies but cannot itself contribute toward interpreting the observed cross-frequency dependencies and their variations among different types of subjects. Our main goal here has been to introduce a novel way to measure dependence and connectivity among fMRI networks, and their transient spectral properties, which resulted in making new observations on the actual nature of the fMRI data. Also subject-wise variation of the measure establishes its advantage in designing new neurophysiological biomarkers in study of human brain. However, more complex designs such as multi-modal or task-based studies is needed to be able to make the observation more interpretable with respect to actual underlying neurophysiological brain activities. For example, there is a possible relation between cross-frequency connectivity observed in this study and the cross-frequency coupling observed in EEG or MEG studies. An interesting question would be if we could trace modulation of well-known

frequency bands of neuronal oscillations in the frequency modes we showed here, A multi-modal study can be performed to shed light on this valid question as a future work.

Finally we need to emphasize that we are not suggesting this method as replacement for existing methods. In fact, we believe there are rich complementarities between cross-frequency and full-spectrum approaches to network connectivity that promise the kind of augmented effectiveness in clinical diagnostic settings.

Appendices

Appendix A

ICA Networks of first set of data

In following we are showing spatial maps of all 50 ICA components identified as intrinsic connectivity networks as explained in section 1.4.1. Sagittal, coronal and axial slices for each SM is shown. More detailed information on these ICNs can be find in supplementary material of [26].

Figure A.1: Sagittal, coronal and axial slices of SMs of ICA components that have been identified as ICNs and have been used in this study. The order that these SMs appear here the same to the order they appear FNCs.

Appendix B

ICA Networks of second set of data

In following we are showing spatial maps of all 47 ICA components identified as intrinsic connectivity networks as explained in section 1.4.1.

Subcortical Networks

Component	Coordinates
Bi substantia nigra	–15, –15, –9
Putamen	24 12,–3 –24, 12, –6
Bi caudate	–9, 18, 0
Globus pallidum	30, –6, 0 –30, –6.3
Bi thalamus	–9, –15, 3

Auditory networks

Component	Coordinates
Superior temporal gyrus	–36, –30, 12 51, –15, 3
Middle temporal gyrus	63, –15, –9 –60, –18, –6

Visual networks

Component	Coordinates
R lingual gyrus	27, –66, –6
Parahippocampal gyrus	–24, –45, –12 30, –45, –12
Middle temporal gyrus	51, –69, 6 –45, –72, 6
Precuneus	30, –78, 33 –27, –78, 27
Frontal gyrus	–30, –93, –6 30, –90, 5
Left lingual gyrus	–9, –78, –6
R cuneus	3, –87, 21
Middle temporal gyrus	54, –51, 12 –54, –51, 9
R cuneus	3, –84, 6
R calcarine gyrus	15, –63, 9
R Superior parietal lobule	–32, –88, –1

Somatomotor networks

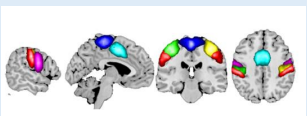

Component	Coordinates
Postcentral gyrus	63, –15, 27 –60, –18, 33
L medial frontal gyrus	42, –21, 54
Right postcentral gyrus	42, –21, 54
L precentral gyrus	–36, –24, 51
Precentral gyrus	54, –6, 27 –54, –9, 30
L SMA	0, 0, 48

Cognitive control networks

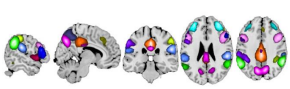

Component	Coordinates
Fusiform gyrus	–42, –57, –12 45, –54, –12
Inferior frontal gyrus	51, 39, 3 –45, 39, 3
Inferior frontal gyrus	33, 24, –6 –33, 24, –6
Supramarginal gyrus	
L precuneus R cingulate gyrus	–6, –72, 39 3, –27, 27
Frontal gyrus	33, 54, 12 –33, 45, 21
Cingulate gyrus	0, –36, 27
Inferior parietal lobule	–42, –42, 45 42, –45, 48
Frontal gyrus	42, 9 30 –45, 12 30
Precuneus	0, –60, 48
Insula	45, –3, 0 –45, 0, 3
Inferior parietal loble	57, –30, 24 –60, –36, 24

Default-mode networks

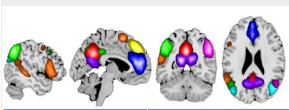

Component	Coordinates
Precuneus	0, –57, 33
L anterior cingulate gyrus	–3, 48, 12
R medial frontal gyrus	3 2042, 45
L angular gyrus	–48, –63, 42
R angular gyrus	51, –60, 39
gyrus	45, –75, 30 –36, –81, 30
L middle temporal gyrus R inferior frontal gyrus	–57, –42, 0 –54, 15 6
L precuneus	–12, –57, 15

Cerebellar networks

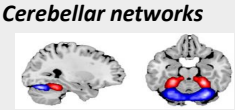

Component	Coordinates
Culmen	–24, –42, –24 27, –48, –24
R declive	30, –75, –24

Figure B.1: Identified ICNs as the subset of ICA components from ICA decomposition of the second set of the data.

Appendix C

Parameter search and performance analysis of WTC

To study performance of our method in compare to wavelet coherence transform implementation of [96] as well as to find the optimal setting in general formulation of wavelet coherence in Equation 3 we simulated pair of time series with dynamic coherence both in time and frequency. 360s long simulated time series are sampled with TR=2s same as fMRI time courses. The pair of time series is correlated at frequency 0.07 Hz during the first third of the duration and at 0.19 Hz during the last third of the duration of the signals. We used sensitivity and specificity as two quantitative measures to study performance of the general wavelet coherence formulation under different settings. As in [50] sensitivity is defined as the ratio of correctly recognized significant coherence to the all truly significant coherence. Specificity is

defined similarly but as the ratio of correctly recognize insignificant coherence to the all truly insignificant coherence. We desire to maximize both at the same time. The significance level was selected as the 90th percentile of null distribution. The null distribution was estimated by surrogating 500 pairs of time series with above properties. Also sensitivity and specificity have been averaged over 500 runs of wavelet coherence analysis. The parameters of Equation 2.6 than we looped through are radius of S and $S^{'}$ along time and frequency dimensions while size of S is always smaller than $S^{'}$ in both dimensions.

Furthermore, in Figure C.2 we show robustness of our optimal parameter search of WTC measure given estimation of SNR of the underlying signal. Looking at the plot, we conclude for the range of displayed SNR (including SNR of conventional fMRI signal) if we find the search for the optimal parameter as above, WTC would be relatively robust to the change in SNR.

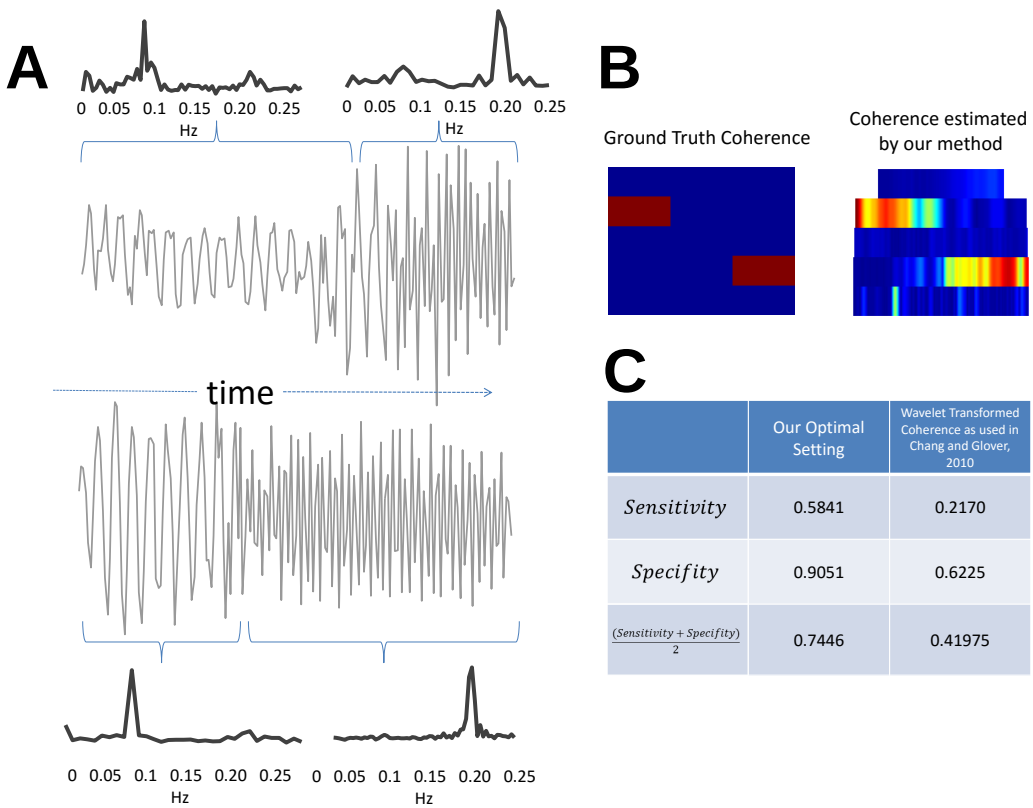

	Our Optimal Setting	Wavelet Transformed Coherence as used in Chang and Glover, 2010
$Sensitivity$	0.5841	0.2170
$Specifity$	0.9051	0.6225
$\frac{(Sensitivity + Specifity)}{2}$	0.7446	0.41975

Figure C.1: Performance optimization of chosen Wavelet Transform Coherence formula and its comparison to the one used in [1]. (A) Simulated input signals. (B) An instance of estimated coherence using the optimal setting along with the ground truth coherence. (C) Comparison to WTC used by [1] with regard to sensitivity and Specifity measures

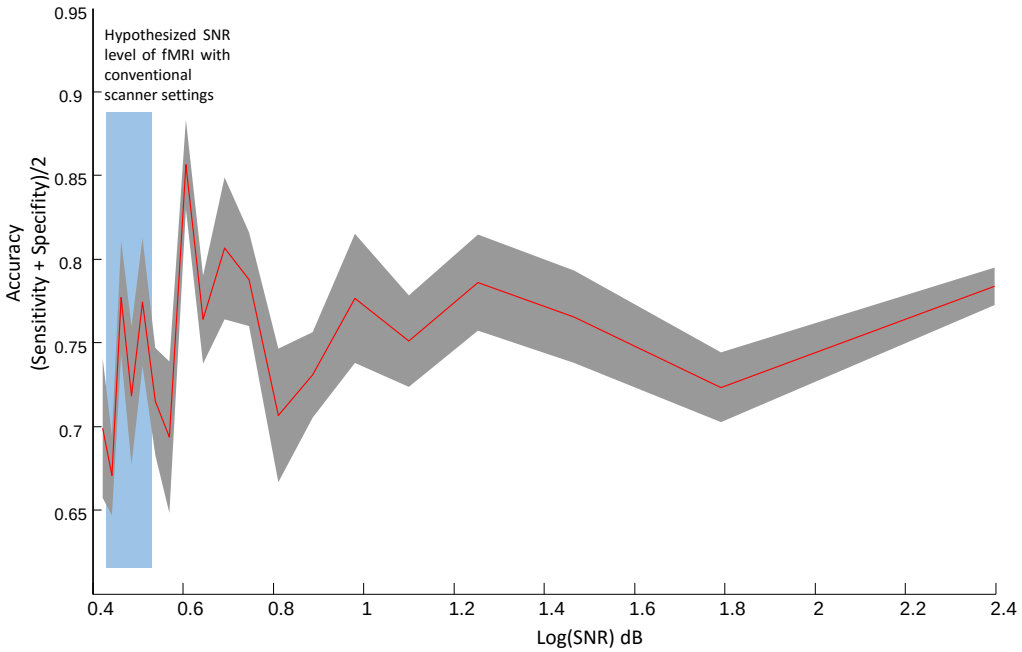

Figure C.2: Accuracy of WTC versus SNR of the simulated pair of signals when for the given SNR, the optimal parameter of WTC is searched for as explained in the text.

Appendix D

Selecting 'K' for k-means clustering

We ran k-means clustering with different number of clusters and observed that by running clustering with enough number of iterations for each choice of 'k', the result cluster centroids are reasonably consistent from low to high model order. Figure D.1 shows k-means centroids for k ranging from 2 to 9. Our choice of 'k' in this study was based on the inspection of f-ratio for each 'k' in the above range. F-ration here is defined as the average ratio of sum of squared distance between each cluster points and the corresponding cluster centroids (inside cluster dispersion) to the sum of square distance of the points outside of the cluster to the same estimated centroids (outside cluster dispersion). We want to minimize this measure with minimum possible number of clusters so we look for 'k's on the elbow of the f-ratio curve which here

is k=5 (Figure D.1 B).

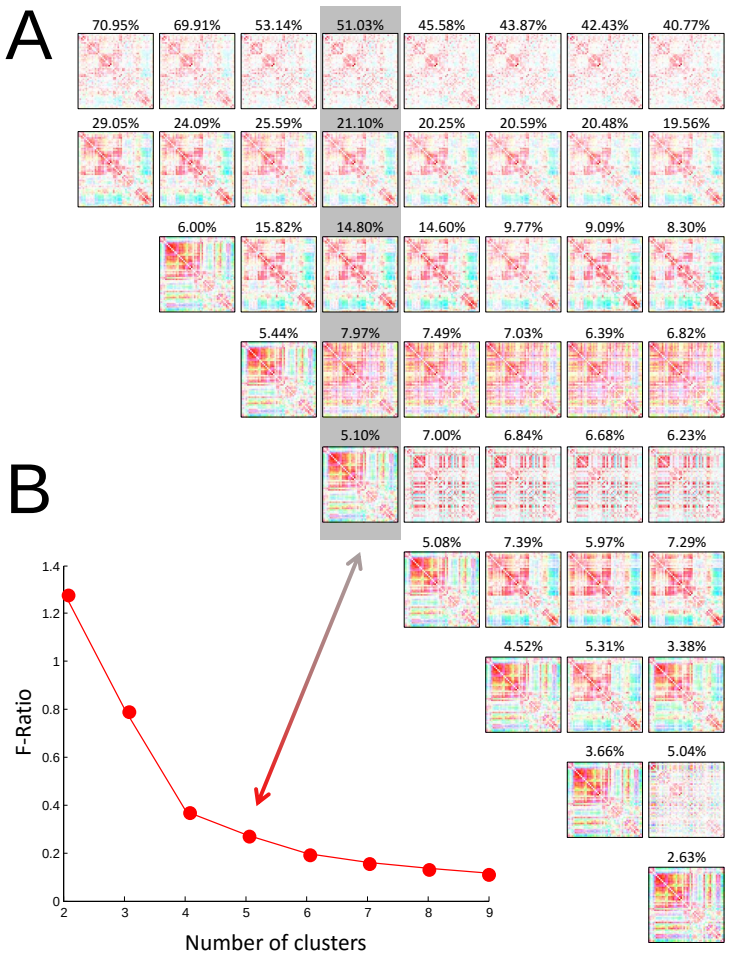

Figure D.1: Analysis for selecting number of cluster for the rest of the study. (A) Result of clustering with different number of clusters for K= 2 through 9 (B) Elbow curve of F-ratio as the measure to choose cluster number (k=5) for the rest of the study.

Appendix E

Cluster visualization in 2-dimensional space

Since we are running k-means on a large number of data point and looking for few centroids, there is a high probability to reach a local minimum solution based on the initial guess and that is the main reason we ran k-means 500 times each with a different initial guess of the solution. In addition to this we also decided to run k-means separately on parts of the data that correspond to different frequency bands. Since we have 5 frequency bands, we would have 25 k-means centroids (5 for each band). By using Sammon non-linear mapping [97] we mapped all 25 centroids into a 2-d plane to get a sense of the space they have spanned. Figure E.1 has summarized this analysis. The bottom side of this hexagon represents centroids of the main k-means clustering. Other sides, each corresponds to single band k-means centroids sorted

by their recurrence rate (1 is the highest recurring centroid and 5 is the lowest one). Inside of the hexagon is the result of Sammon mapping of centroids into a 2-d plane. We can clearly see that main k-means centroids (blue circle) fairly cover the space spanned by other centroids

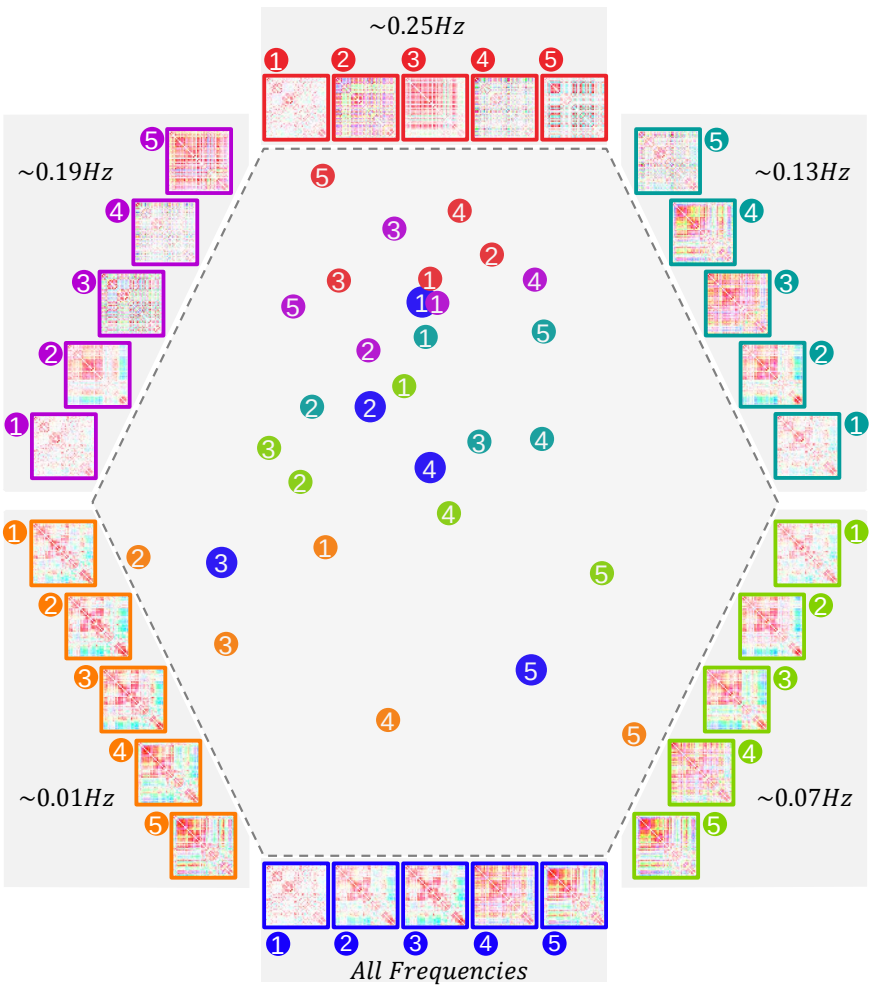

Figure E.1: Nearest neighbor interpolation on cluster labels is used to expand COI of each frequency to span complete duration of scan.

Appendix F

Cone of interest expansion

To accurately account for the occurrence rate of states across frequency band the cone of interests for each band should be expanded (unwarped) to span the whole duration of the scan. The unwarping uses nearest neighbor interpolation on the cluster labels to fit the warped time-frequency plane to a square as follows:

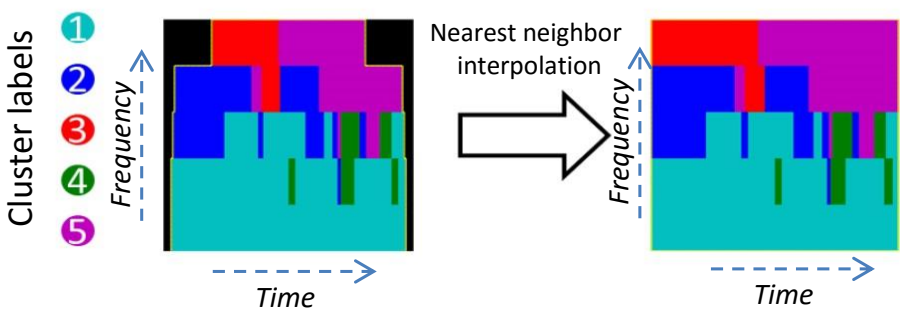

Figure F.1: Nearest neighbor interpolation on cluster labels is used to expand COI of each frequency to span complete duration of scan.

References

[1] C. Chang and G. H. Glover, "Time-frequency dynamics of resting-state brain connectivity measured with fmri," *Neuroimage*, vol. 50, no. 1, pp. 81–98, 2010.

[2] B. Kolb and I. Q. Whishaw, *Fundamentals of human neuropsychology*. Macmillan, 2009.

[3] S. D. Shorvon, "A history of neuroimaging in epilepsy 1909–2009," *Epilepsia*, vol. 50, no. s3, pp. 39–49, 2009.

[4] K. J. Friston, "Functional and effective connectivity in neuroimaging: a synthesis," *Human brain mapping*, vol. 2, no. 1-2, pp. 56–78, 1994.

[5] G. Tononi, O. Sporns, and G. M. Edelman, "A measure for brain complexity: relating functional segregation and integration in the nervous system," *Proceedings of the National Academy of Sciences*, vol. 91, no. 11, pp. 5033–5037, 1994.

[6] E. Oztas, "Neuronal tracing," *Neuroanatomy*, vol. 2, no. 2, 2003.

[7] D. Le Bihan, J.-F. Mangin, C. Poupon, C. A. Clark, S. Pappata, N. Molko, and H. Chabriat, "Diffusion tensor imaging: concepts and applications," *Journal of magnetic resonance imaging*, vol. 13, no. 4, pp. 534–546, 2001.

[8] C. S. Roy and C. S. Sherrington, "On the regulation of the blood-supply of the brain," *The Journal of physiology*, vol. 11, no. 1-2, p. 85, 1890.

[9] L. Pauling and C. D. Coryell, "The magnetic properties and structure of hemoglobin, oxyhemoglobin and carbonmonoxyhemoglobin," *Proceedings of the National Academy of Sciences*, vol. 22, no. 4, pp. 210–216, 1936.

[10] S. A. Huettel, A. W. Song, and G. McCarthy, *Functional magnetic resonance imaging*, vol. 1. Sinauer Associates Sunderland, 2004.

[11] J. Himberg and A. Hyvarinen, "Icasso: Software for investigating the reliability of ica estimates by clustering and visualization," *2003 Ieee Xiii Workshop on Neural Networks for Signal Processing - Nnsp'03*, pp. 259–268, 2003.

[12] E. B. Erhardt, S. Rachakonda, E. J. Bedrick, E. A. Allen, T. Adali, and V. D. Calhoun, "Comparison of multi-subject ica methods for analysis of fmri data," *Human Brain Mapping*, vol. 32, no. 12, pp. 2075–2095, 2011.

[13] E. A. Allen, E. B. Erhardt, E. Damaraju, W. Gruner, J. M. Segall, R. F. Silva, M. Havlicek, S. Rachakonda, J. Fries, R. Kalyanam, A. M. Michael, A. Caprihan, J. A. Turner, T. Eichele, S. Adelsheim, A. D. Bryan, J. Bustillo, V. P. Clark, S. W. Feldstein Ewing, F. Filbey, C. C. Ford, K. Hutchison, R. E. Jung, K. A. Kiehl, P. Kodituwakku, Y. M. Komesu, A. R. Mayer, G. D. Pearlson, J. P. Phillips, J. R. Sadek, M. Stevens, U. Teuscher, R. J. Thoma, and V. D. Calhoun, "A baseline for the multivariate comparison of resting-state networks," *Front Syst Neurosci*, vol. 5, p. 2, 2011.

[14] M. H. Lee, C. D. Smyser, and J. S. Shimony, "Resting-state fmri: a review of methods and clinical applications," *American Journal of Neuroradiology*, vol. 34, no. 10, pp. 1866–1872, 2013.

[15] B. Biswal, F. Z. Yetkin, V. M. Haughton, and J. S. Hyde, "Functional connectivity in the motor cortex of resting human brain using echo-planar mri," *Magnetic Resonance in Medicine*, vol. 34, no. 4, pp. 537–541, 1995.

[16] M. D. Greicius, B. Krasnow, A. L. Reiss, and V. Menon, "Functional connectivity in the resting brain: a network analysis of the default mode hypothesis," *Proc Natl Acad Sci U S A*, vol. 100, no. 1, pp. 253–8, 2003.

[17] C. F. Beckmann, M. DeLuca, J. T. Devlin, and S. M. Smith, "Investigations into resting-state connectivity using independent component analysis," *Philosophical Transactions of the Royal Society B-Biological Sciences*, vol. 360, no. 1457, pp. 1001–1013, 2005.

[18] M. De Luca, C. F. Beckmann, N. De Stefano, P. M. Matthews, and S. M. Smith, "fmri resting state networks define distinct modes of long-distance interactions in the human brain," *Neuroimage*, vol. 29, no. 4, pp. 1359–1367, 2006.

[19] V. D. Calhoun, T. Adali, G. D. Pearlson, and J. J. Pekar, "Spatial and temporal independent component analysis of functional mri data containing a pair of task-related waveforms," *Hum Brain Mapp*, vol. 13, no. 1, pp. 43–53, 2001.

[20] M. Greicius, "Resting-state functional connectivity in neuropsychiatric disorders," *Curr Opin Neurol*, vol. 21, no. 4, pp. 424–30, 2008.

[21] H. Koshino, P. A. Carpenter, N. J. Minshew, V. L. Cherkassky, T. A. Keller, and M. A. Just, "Functional connectivity in an fmri working memory task in high-functioning autism," *Neuroimage*, vol. 24, no. 3, pp. 810–21, 2005.

[22] Q. Yu, J. Sui, S. Rachakonda, H. He, W. Gruner, G. Pearlson, K. A. Kiehl, and V. D. Calhoun, "Altered topological properties

of functional network connectivity in schizophrenia during resting state: a small-world brain network study," *PLoS One*, vol. 6, no. 9, p. e25423, 2011.

[23] R. M. Hutchison, T. Womelsdorf, J. S. Gati, S. Everling, and R. S. Menon, "Resting-state networks show dynamic functional connectivity in awake humans and anesthetized macaques," *Human Brain Mapping*, vol. 34, no. 9, pp. 2154–2177, 2013.

[24] M. Rosenblum, A. Pikovsky, and J. Kurths, "Synchronized firing in coupled inhomogeneous excitable neurons," *Phys. Rev. Lett*, vol. 76, pp. 1804–1807, 1996.

[25] X. Liu and J. H. Duyn, "Time-varying functional network information extracted from brief instances of spontaneous brain activity," *Proceedings of the National Academy of Sciences of the United States of America*, vol. 110, no. 11, pp. 4392–4397, 2013.

[26] E. A. Allen, E. Damaraju, S. M. Plis, E. B. Erhardt, T. Eichele, and V. D. Calhoun, "Tracking whole-brain connectivity dynamics in the resting state," *Cereb Cortex*, 2012.

[27] V. Kiviniemi, T. Vire, J. Remes, A. A. Elseoud, T. Starck, O. Tervonen, and J. Nikkinen, "A sliding time-window ica reveals spatial variability of the default mode network in time," *Brain Connect*, vol. 1, no. 4, pp. 339–47, 2011.

[28] G. D. P. K. A. K. Y. M. W. A. M. M. Sakolu, nal and V. D. Calhoun, "A method for evaluating dynamic functional network connectivity and task-modulation: application to schizophrenia," *Magnetic Resonance Materials in Physics, Biology and Medicine*, vol. 23, no. 5-6, pp. 351–366, 2010.

[29] N. Leonardi, J. Richiardi, M. Gschwind, S. Simioni, J. M. Annoni, M. Schluep, P. Vuilleumier, and D. Van De Ville, "Principal components of functional connectivity: a new approach to study

dynamic brain connectivity during rest," *Neuroimage*, vol. 83, pp. 937–50, 2013.

[30] M. Yaesoubi, R. L. Miller, and V. D. Calhoun, "Mutually temporally independent connectivity patterns: A new framework to study the dynamics of brain connectivity at rest with application to explain group difference based on gender," *NeuroImage*, vol. 107, no. 0, pp. 85–94, 2015.

[31] E. A. Allen, E. Damaraju, S. M. Plis, E. B. Erhardt, T. Eichele, and V. D. Calhoun, "Tracking whole-brain connectivity dynamics in the resting state," *Cerebral Cortex*, vol. 24, no. 3, pp. 663–676, 2014.

[32] A. T. Baria, M. N. Baliki, T. Parrish, and A. V. Apkarian, "Anatomical and functional assemblies of brain bold oscillations," *Journal of Neuroscience*, vol. 31, no. 21, pp. 7910–7919, 2011.

[33] B. Y. J. He, J. M. Zempel, A. Z. Snyder, and M. E. Raichle, "The temporal structures and functional significance of scale-free brain activity," *Neuron*, vol. 66, no. 3, pp. 353–369, 2010.

[34] R. Salvador, A. Martinez, E. Pomarol-Clotet, J. Gomar, F. Vila, S. Sarro, A. Capdevila, and E. T. Bullmore, "A simple view of the brain through a frequency-specific functional connectivity measure," *Neuroimage*, vol. 39, no. 1, pp. 279–289, 2008.

[35] X. N. Zuo, A. Di Martino, C. Kelly, Z. E. Shehzad, D. G. Gee, D. F. Klein, F. X. Castellanos, B. B. Biswal, and M. P. Milham, "The oscillating brain: Complex and reliable," *Neuroimage*, vol. 49, no. 2, pp. 1432–1445, 2010.

[36] V. D. Calhoun, J. Sui, K. Kiehl, J. Turner, E. Allen, and G. Pearlson, "Exploring the psychosis functional connectome: aberrant intrinsic networks in schizophrenia and bipolar disorder," *Front Psychiatry*, vol. 2, p. 75, 2011.

[37] Garrity, "Aberrant 'default mode' functional connectivity in schizophrenia (vol 164, pg 450, 2007)," *American Journal of Psychiatry*, vol. 164, no. 7, pp. 1123–1123, 2007.

[38] D. Cordes, V. M. Haughton, K. Arfanakis, J. D. Carew, P. A. Turski, C. H. Moritz, M. A. Quigley, and M. E. Meyerand, "Frequencies contributing to functional connectivity in the cerebral cortex in "resting-state" data," *American Journal of Neuroradiology*, vol. 22, no. 7, pp. 1326–1333, 2001.

[39] E. Duzel, R. Habib, B. Schott, A. Schoenfeld, N. Lobaugh, A. R. McIntosh, M. Scholz, and H. J. Heinze, "A multivariate, spatiotemporal analysis of electromagnetic time-frequency data of recognition memory," *Neuroimage*, vol. 18, no. 2, pp. 185–197, 2003.

[40] T. Koenig, F. Marti-Lopez, and P. Valdes-Sosa, "Topographic time-frequency decomposition of the eeg," *Neuroimage*, vol. 14, no. 2, pp. 383–90, 2001.

[41] F. Miwakeichi, E. Martinez-Montes, P. A. Valdes-Sosa, N. Nishiyama, H. Mizuhara, and Y. Yamaguchia, "Decomposing eeg data into space-time-frequency components using parallel factor analysis," *Neuroimage*, vol. 22, no. 3, pp. 1035–1045, 2004.

[42] X. P. Song, Y. Zhang, and Y. J. Liu, "Frequency specificity of regional homogeneity in the resting-state human brain," *Plos One*, vol. 9, no. 1, 2014.

[43] S. Mehrkanoon, M. Breakspear, and T. W. Boonstra, "Low-dimensional dynamics of resting-state cortical activity," *Brain Topography*, vol. 27, no. 3, pp. 338–352, 2014.

[44] T. W. Boonstra, A. Daffertshofer, M. Breakspear, and P. J. Beek, "Multivariate time-frequency analysis of electromagnetic brain activity during bimanual. motor learning," *Neuroimage*, vol. 36, no. 2, pp. 370–377, 2007.

[45] J. M. Schoffelen, R. Oostenveld, and P. Fries, "Neuronal coherence as a mechanism of effective corticospinal interaction," *Science*, vol. 308, no. 5718, pp. 111–3, 2005.

[46] E. Damaraju, E. A. Allen, A. Belger, J. M. Ford, S. McEwen, D. H. Mathalon, B. A. Mueller, G. D. Pearlson, S. G. Potkin, A. Preda, J. A. Turner, J. G. Vaidya, T. G. van Erp, and V. D. Calhoun, "Dynamic functional connectivity analysis reveals transient states of dysconnectivity in schizophrenia," *Neuroimage Clin*, vol. 5, pp. 298–308, 2014.

[47] B. Rashid, E. Damaraju, G. D. Pearlson, and V. D. Calhoun, "Dynamic connectivity states estimated from resting fmri identify differences among schizophrenia, bipolar disorder, and healthy control subjects," *Frontiers in Human Neuroscience*, vol. 8, 2014.

[48] P. D. Welch, "The use of fast fourier transform for the estimation of power spectra: A method based on time averaging over short, modified periodograms," *Audio and Electroacoustics, IEEE Transactions on*, vol. 15, no. 2, pp. 70–73, 1967.

[49] C. Torrence and G. P. Compo, "A practical guide to wavelet analysis," *Bulletin of the American Meteorological Society*, vol. 79, no. 1, pp. 61–78, 1998.

[50] S. Mehrkanoon, M. Breakspear, A. Daffertshofer, and T. Boonstra, "Generalized time-frequency coherency for assessing neural interactions in electrophysiological recordings," in *Nature Precedings*, 2011.

[51] M. J. Jafri, G. D. Pearlson, M. Stevens, and V. D. Calhoun, "A method for functional network connectivity among spatially independent resting-state components in schizophrenia," *Neuroimage*, vol. 39, no. 4, pp. 1666–1681, 2008.

[52] D. Bhugra, "The global prevalence of schizophrenia," *PLoS Med*, vol. 2, no. 5, p. e151; quiz e175, 2005. Bhugra, Dinesh eng Comment 2005/05/27 09:00 PLoS Med. 2005 May;2(5):e151; quiz e175. Epub 2005 May 31.

[53] M. S. Keshavan, B. A. Clementz, G. D. Pearlson, J. A. Sweeney, and C. A. Tamminga, "Reimagining psychoses: An agnostic approach to diagnosis," *Schizophrenia Research*, vol. 146, no. 1-3, pp. 10–16, 2013.

[54] E. Cheniaux, J. Landeira-Femandez, L. L. Telles, J. L. M. Lessa, A. Dias, T. Duncan, and M. Versiani, "Does schizoaffective disorder really exist? a systematic review of the studies that compared schizoaffective disorder with schizophrenia or mood disorders," *Journal of Affective Disorders*, vol. 106, no. 3, pp. 209–217, 2008.

[55] R. Kotov, S. H. Leong, R. Mojtabai, A. C. E. Erlanger, L. J. Fochtmann, E. Constantino, G. A. Carlson, and E. J. Bromet, "Boundaries of schizoaffective disorder revisiting kraepelin," *Jama Psychiatry*, vol. 70, no. 12, pp. 1276–1286, 2013.

[56] S. K. Schultz and N. C. Andreasen, "Schizophrenia," *Lancet*, vol. 353, no. 9162, pp. 1425–30, 1999. Schultz, S K Andreasen, N C eng Review ENGLAND London, England 1999/05/05 Lancet. 1999 Apr 24;353(9162):1425-30.

[57] N. C. Andreasen and M. Flaum, "Schizophrenia: the characteristic symptoms," *Schizophr Bull*, vol. 17, no. 1, pp. 27–49, 1991.

[58] A. Fornito, A. Zalesky, C. Pantelis, and E. T. Bullmore, "Schizophrenia, neuroimaging and connectomics," *Neuroimage*, vol. 62, no. 4, pp. 2296–2314, 2012.

[59] K. J. Friston, "The disconnection hypothesis," *Schizophr Res*, vol. 30, no. 2, pp. 115–25, 1998.

[60] W. Pettersson-Yeo, P. Allen, S. Benetti, P. McGuire, and A. Mechelli, "Dysconnectivity in schizophrenia: Where are we now?," *Neuroscience and Biobehavioral Reviews*, vol. 35, no. 5, pp. 1110–1124, 2011.

[61] C. Wernicke, *Grundriss der Psychiatrie in klinischen Vorlesungen.* 1906.

[62] J. S. Damoiseaux and M. D. Greicius, "Greater than the sum of its parts: a review of studies combining structural connectivity and resting-state functional connectivity," *Brain Struct Funct*, vol. 213, no. 6, pp. 525–33, 2009.

[63] J. H. Xiong, L. M. Parsons, J. H. Gao, and P. T. Fox, "Interregional connectivity to primary motor cortex revealed using mri resting state images," *Human Brain Mapping*, vol. 8, no. 2-3, pp. 151–156, 1999.

[64] D. A. Gusnard, E. Akbudak, G. L. Shulman, and M. E. Raichle, "Medial prefrontal cortex and self-referential mental activity: relation to a default mode of brain function," *Proc Natl Acad Sci U S A*, vol. 98, no. 7, pp. 4259–64, 2001.

[65] L. A. Flashman, *Disorders of insight, self-awareness, and attribution in schizophrenia.* New York: W.W. Norton & Co, 2004.

[66] R. L. Bluhm, J. Miller, R. A. Lanius, E. A. Osuch, K. Boksman, R. W. Neufeld, J. Theberge, B. Schaefer, and P. Williamson, "Spontaneous low-frequency fluctuations in the bold signal in schizophrenic patients: anomalies in the default network," *Schizophr Bull*, vol. 33, no. 4, pp. 1004–12, 2007.

[67] K. J. Friston and C. D. Frith, "Schizophrenia: a disconnection syndrome?," *Clin Neurosci*, vol. 3, no. 2, pp. 89–97, 1995.

[68] S. Whitfield-Gabrieli, H. W. Thermenos, S. Milanovic, M. T. Tsuang, S. V. Faraone, R. W. McCarley, M. E. Shenton, A. I.

Green, A. Nieto-Castanon, P. LaViolette, J. Wojcik, J. D. Gabrieli, and L. J. Seidman, "Hyperactivity and hyperconnectivity of the default network in schizophrenia and in first-degree relatives of persons with schizophrenia," *Proc Natl Acad Sci U S A*, vol. 106, no. 4, pp. 1279–84, 2009.

[69] Y. Zhou, M. Liang, L. X. Tian, K. Wang, Y. H. Hao, H. H. Liu, Z. N. Liu, and T. Z. Jiang, "Functional disintegration in paranoid schizophrenia using resting-state fmri," *Schizophrenia Research*, vol. 97, no. 1-3, pp. 194–205, 2007.

[70] R. Yu, Y. L. Chien, H. L. Wang, C. M. Liu, C. C. Liu, T. J. Hwang, M. H. Hsieh, H. G. Hwu, and W. Y. Tseng, "Frequency-specific alternations in the amplitude of low-frequency fluctuations in schizophrenia," *Hum Brain Mapp*, vol. 35, no. 2, pp. 627–37, 2014.

[71] S. A. Meda, Z. Wang, E. I. Ivleva, G. Poudyal, M. S. Keshavan, C. A. Tamminga, J. A. Sweeney, B. A. Clementz, D. J. Schretlen, V. D. Calhoun, S. Lui, E. Damaraju, and G. D. Pearlson, "Frequency-specific neural signatures of spontaneous low-frequency resting state fluctuations in psychosis: Evidence from bipolar-schizophrenia network on intermediate phenotypes (b-snip) consortium," *Schizophr Bull*, 2015.

[72] M. J. Hoptman, X. N. Zuo, P. D. Butler, D. C. Javitt, D. D'Angelo, C. J. Mauro, and M. P. Milham, "Amplitude of low-frequency oscillations in schizophrenia: a resting state fmri study," *Schizophr Res*, vol. 117, no. 1, pp. 13–20, 2010.

[73] N. D. Woodward, H. Karbasforoushan, and S. Heckers, "Thalamocortical dysconnectivity in schizophrenia," *Am J Psychiatry*, vol. 169, no. 10, pp. 1092–9, 2012.

[74] A. Anticevic, M. W. Cole, G. Repovs, J. D. Murray, M. S. Brumbaugh, A. M. Winkler, A. Savic, J. H. Krystal, G. D. Pearlson,

and D. C. Glahn, "Characterizing thalamo-cortical disturbances in schizophrenia and bipolar illness," *Cereb Cortex*, vol. 24, no. 12, pp. 3116–30, 2014.

[75] M. Liang, Y. Zhou, T. Jiang, Z. Liu, L. Tian, H. Liu, and Y. Hao, "Widespread functional disconnectivity in schizophrenia with resting-state functional magnetic resonance imaging," *Neuroreport*, vol. 17, no. 2, pp. 209–13, 2006.

[76] S. A. Meda, A. Gill, M. C. Stevens, R. P. Lorenzoni, D. C. Glahn, V. D. Calhoun, J. A. Sweeney, C. A. Tamminga, M. S. Keshavan, G. Thaker, and G. D. Pearlson, "Differences in resting-state functional magnetic resonance imaging functional network connectivity between schizophrenia and psychotic bipolar probands and their unaffected first-degree relatives," *Biol Psychiatry*, vol. 71, no. 10, pp. 881–9, 2012.

[77] J. Lisman, "The theta/gamma discrete phase code occuring during the hippocampal phase precession may be a more general brain coding scheme," *Hippocampus*, vol. 15, no. 7, pp. 913–922, 2005.

[78] M. X. Cohen, N. Axmacher, D. Lenartz, C. E. Elger, V. Sturm, and T. E. Schlaepfer, "Good vibrations: cross-frequency coupling in the human nucleus accumbens during reward processing," *Journal of Cognitive Neuroscience*, vol. 21, no. 5, pp. 875–889, 2009.

[79] J. Lisman and M. Idiart, "Storage of 7 +/- 2 short-term memories in oscillatory subcycles," *Science*, vol. 267, no. 5203, pp. 1512–1515, 1995.

[80] H. Berendse, J. Verbunt, P. Scheltens, B. van Dijk, and E. Jonkman, "Magnetoencephalographic analysis of cortical activity in alzheimer's disease: a pilot study," *Clinical Neurophysiology*, vol. 111, no. 4, pp. 604 – 612, 2000.

[81] P. L. Nunez, R. B. Silberstein, Z. Shi, M. R. Carpenter, R. Srinivasan, D. M. Tucker, S. M. Doran, P. J. Cadusch, and R. S. Wijesinghe, "Eeg coherency ii: experimental comparisons of multiple measures," *Clinical Neurophysiology*, vol. 110, no. 3, pp. 469 – 486, 1999.

[82] C. Besthorn, H. Frstl, C. Geiger-Kabisch, H. Sattel, T. Gasser, and U. Schreiter-Gasser, "Eeg coherence in alzheimer disease," *Electroencephalography and Clinical Neurophysiology*, vol. 90, no. 3, pp. 242 – 245, 1994.

[83] C. E. Schroeder and P. Lakatos, "Low-frequency neuronal oscillations as instruments of sensory selection," *Trends in neurosciences*, vol. 32, no. 1, pp. 9–18, 2009.

[84] J. M. Palva, S. Palva, and K. Kaila, "Phase synchrony among neuronal oscillations in the human cortex," *The Journal of Neuroscience*, vol. 25, no. 15, pp. 3962–3972, 2005.

[85] P. R. Shirvalkar, P. R. Rapp, and M. L. Shapiro, "Bidirectional changes to hippocampal theta–gamma comodulation predict memory for recent spatial episodes," *Proceedings of the National Academy of Sciences*, vol. 107, no. 15, pp. 7054–7059, 2010.

[86] J. M. Palva, S. Monto, S. Kulashekhar, and S. Palva, "Neuronal synchrony reveals working memory networks and predicts individual memory capacity," *Proceedings of the National Academy of Sciences*, vol. 107, no. 16, pp. 7580–7585, 2010.

[87] C. Stam, "Nonlinear dynamical analysis of {EEG} and meg: Review of an emerging field," *Clinical Neurophysiology*, vol. 116, no. 10, pp. 2266 – 2301, 2005.

[88] R. T. Canolty and R. T. Knight, "The functional role of cross-frequency coupling," *Trends Cogn Sci*, vol. 14, no. 11, pp. 506–15, 2010.

[89] M. Lowe, B. Mock, and J. Sorenson, "Functional connectivity in single and multislice echoplanar imaging using resting-state fluctuations," *NeuroImage*, vol. 7, no. 2, pp. 119 – 132, 1998.

[90] M. W. Cole, S. Pathak, and W. Schneider, "Identifying the brain's most globally connected regions," *Neuroimage*, vol. 49, no. 4, pp. 3132–3148, 2010.

[91] M. Ystad, E. Hodneland, S. Adolfsdottir, J. Haasz, A. J. Lundervold, T. Eichele, and A. Lundervold, "Cortico-striatal connectivity and cognition in normal aging: A combined dti and resting state fmri study," *Neuroimage*, vol. 55, no. 1, pp. 24–31, 2011.

[92] W. R. Shirer, S. Ryali, E. Rykhlevskaia, V. Menon, and M. D. Greicius, "Decoding subject-driven cognitive states with whole-brain connectivity patterns," *Cereb Cortex*, vol. 22, no. 1, pp. 158–65, 2012.

[93] E. Tagliazucchi, F. von Wegner, A. Morzelewski, V. Brodbeck, and H. Laufs, "Dynamic bold functional connectivity in humans and its electrophysiological correlates," *Front Hum Neurosci*, vol. 6, p. 339, 2012.

[94] N. E. Huang, Z. Shen, S. R. Long, M. L. C. Wu, H. H. Shih, Q. N. Zheng, N. C. Yen, C. C. Tung, and H. H. Liu, "The empirical mode decomposition and the hilbert spectrum for nonlinear and non-stationary time series analysis," *Proceedings of the Royal Society a-Mathematical Physical and Engineering Sciences*, vol. 454, no. 1971, pp. 903–995, 1998.

[95] A. Bruns, "Fourier-, hilbert- and wavelet-based signal analysis: are they really different approaches?," *Journal of Neuroscience Methods*, vol. 137, no. 2, pp. 321–332, 2004. 845KZ Times Cited:127 Cited References Count:20.

[96] A. Grinsted, J. C. Moore, and S. Jevrejeva, "Application of the cross wavelet transform and wavelet coherence to geophysical

time series," *Nonlinear Processes in Geophysics*, vol. 11, no. 5-6, pp. 561–566, 2004.

[97] J. W. Sammon, "A nonlinear mapping for data structure analysis," *Ieee Transactions on Computers*, vol. C 18, no. 5, pp. 401–&, 1969.